Ore Geology Reviews 135 (2021) 104197

Contents lists available at ScienceDirect

Ore Geology Reviews

journal homepage: www.elsevier.com/locate/oregeorev

Genesis of highly fractionated granite and associated W-Sn-Be mineralization in the Xuebaoding area, Sichuan Province, China

Yongwang Zhang [a,b,*], Yan Liu [c,*], Xinxiang Zhu [c], Markus B. Raschke [d], Nengping Shen [e]

[a] State Key Laboratory of Petroleum Resources and Prospecting, China University of Petroleum, Beijing 102249, China
[b] College of Geosciences, China University of Petroleum, Beijing 102249, China
[c] Key Laboratory of Deep-Earth Dynamics of Ministry of Natural Resources, Institute of Geology, Chinese Academy of Geological Science, Beijing 100037, China
[d] Department of Physics, University of Colorado, Boulder, CO 80303, USA
[e] State Key Laboratory of Ore Deposit Geochemistry, Institute of Geochemistry, Chinese Academy of Sciences, Guiyang 550081, China

ARTICLE INFO

Keywords:
Highly fractionated granite
B isotopes
W–Sn–Be mineralization
Sichuan Province
S-type granite

ABSTRACT

The Xuebaoding W–Sn–Be deposit in the Songpan–Garzê Orogenic Belt of western China contains coarse-grained W–Sn–Be–F–P-bearing minerals, and has been the subject of several previous geochronological, petrographic, and ore-forming fluid studies. However, the genesis of the deposit, including the Pankou and Pukouling granites and associated W–Sn–Be mineralization has remained unclear. In this study, geochemical and Sr–Nd–Pb isotope analyses of both Pankou and Pukouling granites were performed revealing high A/CNK values (>1.09) and alkali contents (8.16–13.01 wt%), and are enriched in W, Sn, Be, B, F and volatiles. Sr–Nd–Pb isotope values of $^{87}Sr/^{86}Sr_{(i)}$ = 0.67–0.73, $\varepsilon_{Nd}(t)$ = − 11.49 to − 23.19, $^{206}Pb/^{204}Pb$ = 18.710–19.908, $^{207}Pb/^{204}Pb$ = 15.647–15.708, and $^{208}Pb/^{204}Pb$ = 38.434–38.929 were determined. The samples contain 30–35 vol% muscovite and no hornblende. In addition, the granites have high Be (6.73–1681 ppm), Sn (28.9–200 ppm), and W (2.07–54.1 ppm) contents, and the host marble has low and variable Be (0.05–0.21 ppm), Sn (0.23–0.82 ppm), and W (0.20–2.37 ppm) contents. Further, three types of tourmaline were identified as associated with the magmatic–hydrothermal stage of the granites, with B isotope values of − 11.21‰ to − 13.65‰, also indicating a metasedimentary origin for the granites. All these results indicate that the Pankou and Pukouling granites show highly fractionated S-type characters, derived by partial melting of metasedimentary rocks. Thus, the W–Sn–Be mineralization was closely related to the evolution of such highly fractionated granites in Xuebaoding.

1. Introduction

The Xuebaoding deposit contains euhedral, gem quality, and coarse-grained beryl, scheelite, cassiterite, apatite, fluorite, and muscovite crystals. The deposit is located 5 km southeast of Mt. Xuebaoding (5,588 m) at an altitude of 4,000–4,300 m, and is 14.5 km northwest of Huya town in Sichuan Province, southwest China. Due to its unusual W–Sn–Be-bearing mineral assemblages, the Xuebaoding deposit and the host Pankou and Pukouling granites have been the subject of significant research (Cao et al., 2002, 2004; Li et al., 2007; Liu et al., 2007a, 2010; 2007b; 2007c; 2011a, b; Liu, 2010; Rakovan, 2007; Zhang et al., 2014; Liu et al., 2017). Notably, Xuebaoding deposit is the only W–Sn–Be deposit in the Songpan–Garzê Orogenic Belt (Fig. 1), which contrasts with the common occurrence of large W–Sn deposits in Nanling in South China (Mao et al., 2019).

Most W–Sn deposits worldwide are associated with granitic intrusions, and dominated by scheelite, disseminated cassiterite, and minor beryl, with skarn- and greisen-type alteration (Anglin et al., 1996; Brugger et al., 2002; Lu et al., 2003; Somarin and Ashley, 2004; Bettencourt et al., 2005; Gu et al., 2006; Macey and Harris, 2006; Pal et al., 2007; Neiva, 2008; Mao et al., 2019). However, large beryl crystals often occur in pegmatite deposits and, to a lesser extent, in hydrothermal deposits (Groat et al., 2002, 2008; Lu et al., 2003; Marshall et al., 2003, 2004; Gavrilenko et al., 2006; Vapnik et al., 2006), such as the Keketuohai No. 3 pegmatite in Xinjiang (Aurisicchio et al., 1988; Wang et al., 2009). The association of W, Sn, and Be mineralization of scheelite, cassiterite, and beryl, with less alteration in the Pankou and Pukouling granites in the Xuebaoding deposit is unusual (Yokart et al., 2003; Somarin and Ashley, 2004; Bettencourt et al., 2005; Esmaeily et al., 2005; Pettke et al., 2005; Macey and Harris, 2006; Neiva, 2008; Liu

* Corresponding authors.
E-mail addresses: zhangyw@cup.edu.cn (Y. Zhang), ly@cags.ac.cn (Y. Liu).

https://doi.org/10.1016/j.oregeorev.2021.104197
Received 29 December 2020; Received in revised form 15 April 2021; Accepted 25 April 2021
Available online 28 April 2021

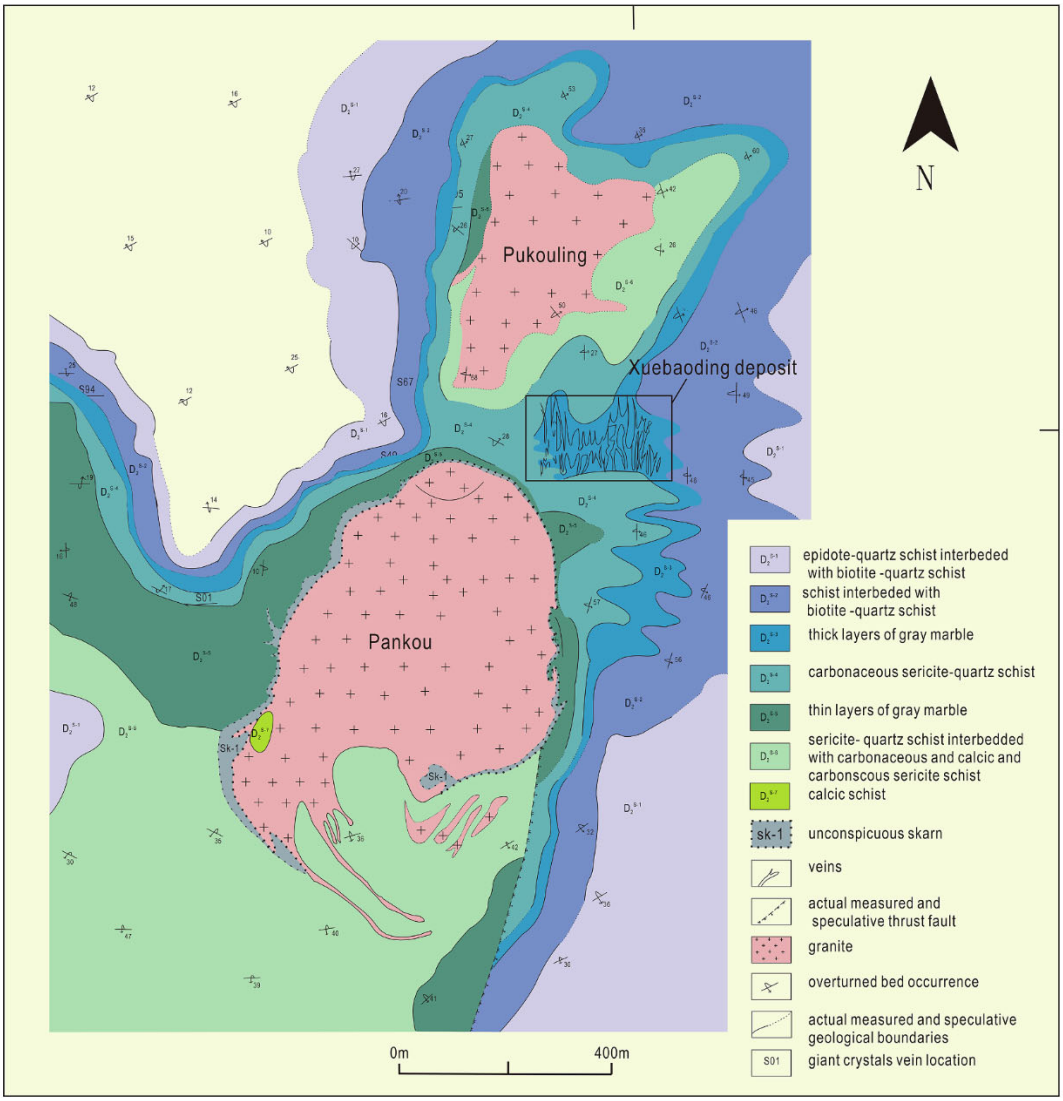

Fig. 1. Simplified regional geological map of the Pankou and Pukouling granites, which are associated with W–Sn–Be vein and pod mineralization in surrounding Upper Triassic marble. Figure modified after Geology and Mineral Resource Bureau of Sichuan Province (1975).

et al., 2012a, b).

Previous studies have focused mainly on the ages, major and trace element features of the Pankou and Pukouling granites, as well as the characteristics of the ore-forming fluids. However, few studies have investigated the petrogenesis of the granitic intrusions and their roles in W–Sn–Be mineralization (Wang et al., 2013; Liu et al., 2016; Wu et al., 2017). In particular, the lack of strong alteration in the deposit is unusual (Liu et al., 2011a, 2017) and distinctive from typical skarn- or greisen-type mineralization in granitic W–Sn deposits.

Tourmaline is a useful mineral indicator in metamorphic and hydrothermal systems, because it has a variable chemical composition that is responsive to the local geochemical environment during crystal growth. In hydrothermal ore deposits, the composition of tourmaline is controlled by temperature, pressure, and the fluid and host rock composition. Thus, B isotopes can trace its source, because tourmaline is the only borosilicate mineral in common types of rock (Samson and Sinclair, 1992; Rozendaal and Bruwer, 1995; Jiang et al., 2008; Garda et al., 2009; Longfellow and Swanson, 2011; Drivenes et al., 2015; Huang et al., 2016). In the Xuebaoding deposit, three types of tourmalines have been identified: disseminated tourmaline in the granite (type I), tourmaline clusters at the margin of the granite (type II), and tourmaline in mineralized veins (type III; Zhu et al., 2020). Based on geochemical features, type I and II tourmalines can be classified as the dravite–schorl solid solution, whereas type III tourmaline corresponds to foitite and schorl. The crystallization sequence of the three tourmalines is: (1) type II skeletal tourmalines formed first from undercooled melt; (2) type I tourmaline formed from an immiscible B-rich aqueous fluid during the late stage of granite crystallization; and (3) type III tourmaline crystallized in the mineralized veins from magmatic–hydrothermal fluids (Fig. 2). Type I tourmalines always coexist with albite and muscovite rather than K-feldspar. The type I tourmaline crystals are poorly zoned and ~ 200 μm in diameter (Fig. 2A–C). Scheelite grains that are about 10 μm in size generally occur in fractures in muscovite (Fig. 2A, C). Type II tourmaline crystals are 1–2 cm in size and always coexist with albite, K-feldspar, and muscovite (Fig. 2D–E). Such type II tourmalines have a skeletal texture, which comprises numerous small (50–150 μm) disconnected, fine-grained, tourmaline crystals (Fig. 2E–F). The coarse-grained type III tourmalines (2–5 cm) always coexist with albite and K-feldspar (Fig. 2F) in the mineralized veins.

In this study, we present detailed petrographic observations, geochemical and Sr–Nd–Pb isotopic data for the granites and B isotope data for tourmaline in order to constrain the genesis of the Pankou and Pukouling granites, and their roles in the formation of the Xuebaoding W–Sn–Be deposit.

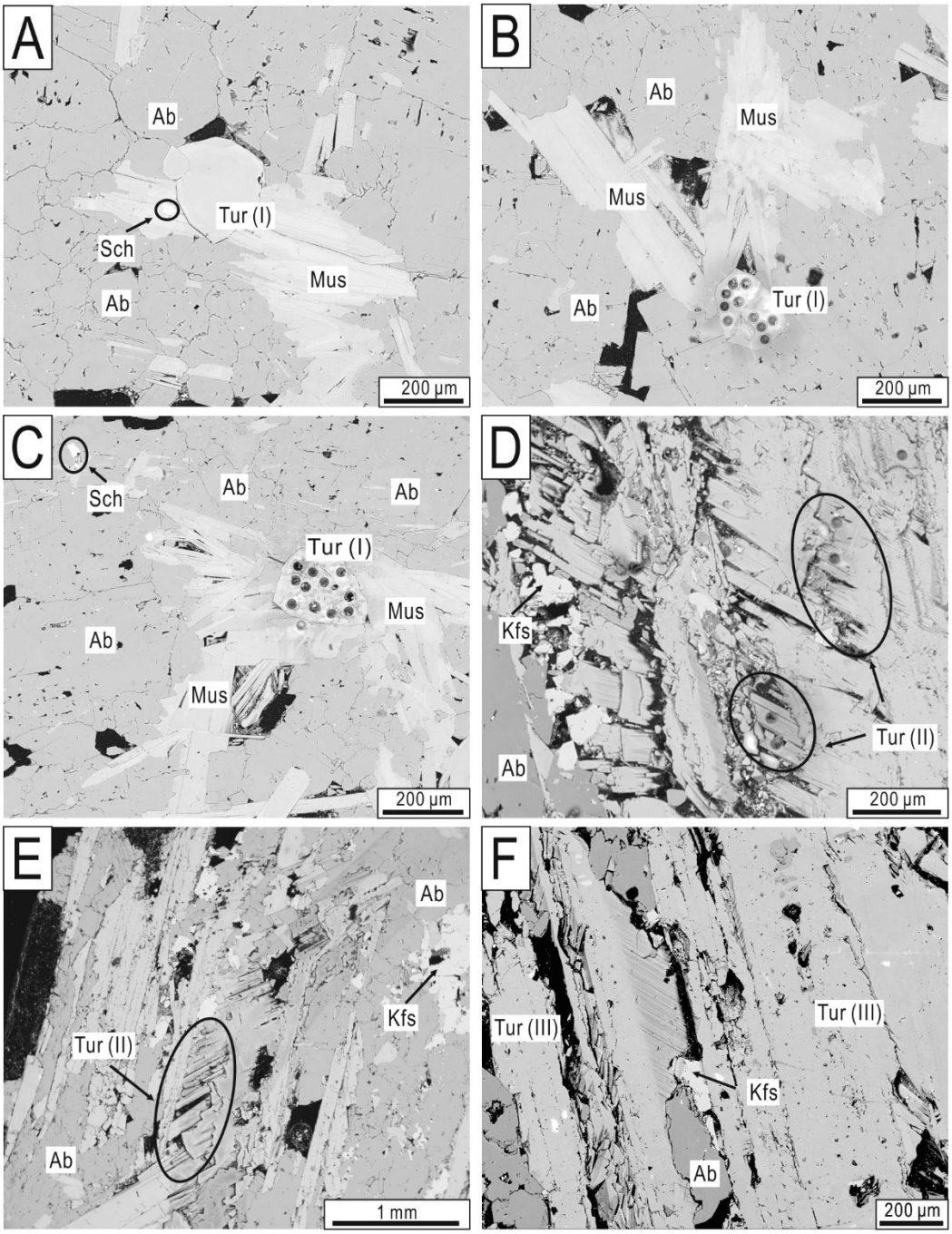

Fig. 2. Back-scattered electron images of tourmalines from the Xuebaoding deposit. (A–C) In the Pankou and Pukouling granites, type I tourmaline is euhedral and staying with muscovite and albite. Muscovite and albite were overlapped by fine-grained scheelite. (D–E) radial clusters of skeletal type II tourmaline intergrown with albite and K-feldspar in an ore vein. (F) Albite and fine-grained K-feldspar occurred in fissures of type III tourmaline crystals.

2. Geological setting and sample petrography

The Xuebaoding deposit is located in the Pankou Dome of the western Yangtze Block (Fig. 1). The Pankou and Pukouling granites intruded Triassic sedimentary rocks (Fig. 1) in the core of the Pankou anticline. The Pankou and Pukouling granites consist of quartz (35–40 vol%), albite (30–35 vol%), muscovite (30–35 vol%), and minor K-feldspar (0–5 vol%) and mafic minerals. Accessory minerals include zircon, apatite, pyrite, rutile, limonite, scheelite, tourmaline, and cassiterite. The Pankou and Pukouling granites are assumed to have been the main source of fluids and materials for the Xuebaoding deposit, and were emplaced at a shallow crustal level into marble and schist. Zircons in both granites have experienced radiation damage and contain U-bearing mineral inclusions, similar to zircons in other W–Sn-mineralized granites (Wang et al., 2013, 2014). As such, zircon ages are unreliable and muscovite $^{40}Ar/^{39}Ar$ dating has been used to date the granites. Muscovite $^{40}Ar/^{39}Ar$ dating of the Pukouling and Pankou granites has yielded inverse isochron ages of 200.6 ± 1.2 Ma and 193.7 ± 1.1 Ma, respectively (Liu et al., 2010). Other dating results for the granites and Xuebaoding deposit include: (1) a quartz $^{40}Ar/^{39}Ar$ age of 191.8 ± 0.7 Ma (Cao et al., 2002); (2) a muscovite $^{40}Ar/^{39}Ar$ plateau age of 189.9 ± 1.8 Ma; (3) a Sm–Nd isochron age for scheelite of 182.0 ± 9.2 Ma (Liu et al., 2007a); (4) an *in situ* U–Pb age for cassiterite of 194.8 ± 6.2 Ma and 194.8 ± 6.4 Ma (Zhang et al., 2014); (5) an $^{40}Ar/^{39}Ar$ age for

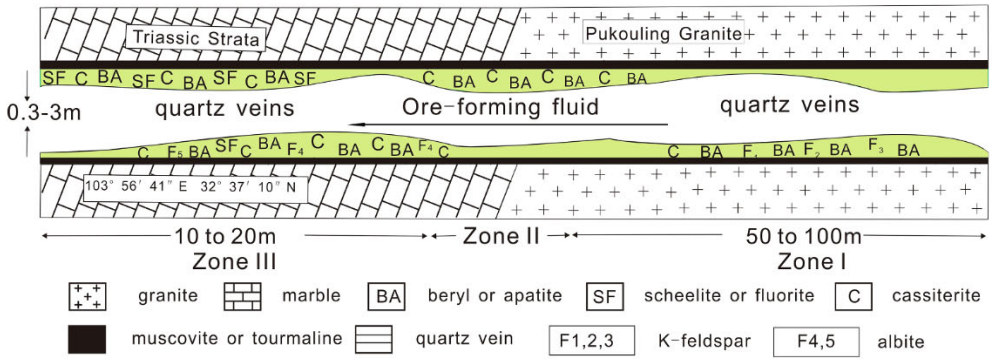

Fig. 3. Schematic cross-section of a typical mineralized vein at the transition from granite to marble/schist showing the distribution of beryl, cassiterite, scheelite, muscovite, tourmaline, albite, and K-feldspar, and the host rock transition from granite to Triassic metamorphic rocks, which is divided into three characteristic zones (modified after Liu et al., 2010). Mineral abbreviations: Ab = albite, Kf = K-feldspar, Mu = muscovite, and Qz = quartz.

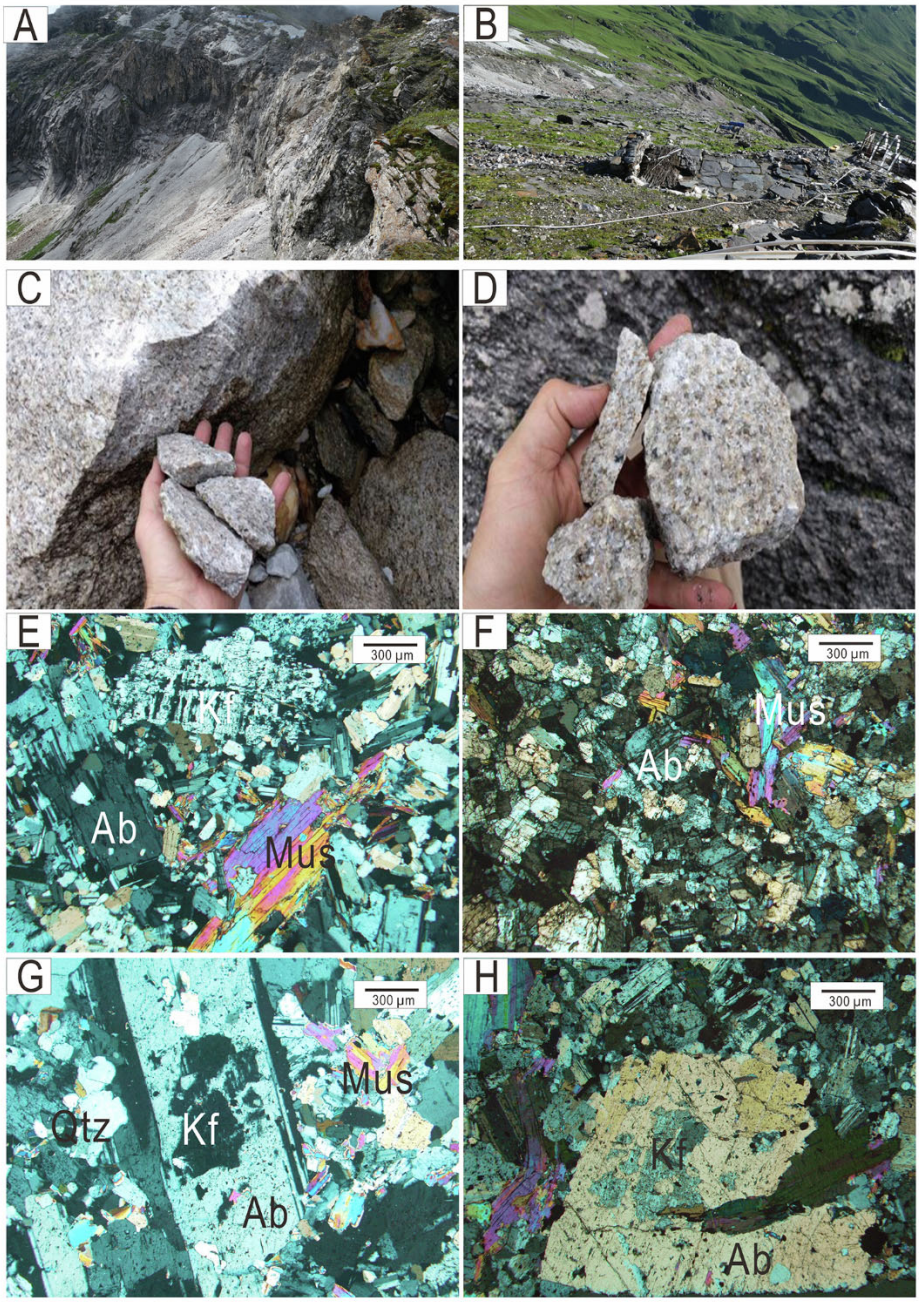

Fig. 4. (A) Photograph of outcrops of Pankou granite in a cirque, with mines in the marble bands above the granite. The Pukouling granite crops out to the right over the ridge. The two granite outcrops of the Pankou and Pukou granites are in cirques separated by a ridge of marble and schist. (B) Photograph of the Pukouling granite above the Pankou granite, along with the bordering marble band. (C–D) Hand specimens of the Pankou and Pukouling granites. (E–F) Photomicrographs in cross-polarized light of the main rock-forming minerals (muscovite, albite, and quartz) in the Pankou and Pukouling granites, which also exhibit (G–H) albitization of K-feldspar. E-H from Liu (2010).

Table 1
EMPA results of albite as rock-forming mineral in Pankou granites, Xuebaoding deposit.

Samples	Ab1	Ab2	Ab3	Ab4	Ab5	Ab6
Na_2O	11.02	10.84	10.80	10.86	10.95	11.53
MgO	0.00	0.00	0.00	0.00	0.00	0.00
Al_2O_3	18.74	18.49	19.03	18.74	18.62	18.81
SiO_2	70.04	70.38	69.35	69.57	70.24	69.15
K_2O	0.01	0.06	0.16	0.11	0.08	0.17
CaO	0.15	0.08	0.46	0.49	0.00	0.31
TiO_2	0.03	0.05	0.09	0.09	0.03	0.00
Cr_2O_3	0.00	0.02	0.07	0.00	0.00	0.00
MnO	0.00	0.00	0.00	0.14	0.00	0.00
FeO	0.00	0.00	0.00	0.00	0.00	0.00
NiO	0.00	0.08	0.04	0.00	0.08	0.03
Total	99.99	100.00	100.00	100.00	100.00	100.00
Si	3.04	3.06	3.02	3.03	3.05	3.02
Al	0.96	0.95	0.98	0.96	0.95	0.97
Ca	0.01	0.00	0.02	0.02	0.00	0.01
Na	0.93	0.91	0.91	0.92	0.92	0.98
K	0.00	0.00	0.01	0.01	0.00	0.01
Ba	0.00	0.00	0.00	0.00	0.00	0.00
An	0.75	0.40	2.28	2.42	0.00	1.45
Ab	99.19	99.23	96.78	96.94	99.52	97.60
Or	0.06	0.36	0.94	0.65	0.48	0.95

(data from Liu (2010))

Table 2
EMPA results of K-feldspar as rock-forming mineral in Pankou granites, Xuebaoding deposit.

Samples	fd1	fd2	fd3	fd4	fd5	fd6
Na_2O	0.35	0.33	0.27	0.21	0.30	0.28
MgO	0.00	0.00	0.01	0.00	0.04	0.00
Al_2O_3	17.36	17.54	17.48	17.34	17.66	17.47
SiO_2	65.88	66.10	66.07	65.85	65.88	66.06
K_2O	15.97	15.93	15.81	15.59	15.76	16.02
CaO	0.00	0.10	0.08	0.00	0.02	0.00
TiO_2	0.00	0.00	0.07	0.00	0.04	0.00
Cr_2O_3	0.03	0.00	0.03	0.83	0.16	0.00
MnO	0.00	0.00	0.03	0.16	0.01	0.02
FeO	0.14	0.00	0.05	0.03	0.08	0.16
NiO	0.27	0.00	0.10	0.00	0.04	0.00
Total	100.00	100.00	100.00	100.01	99.99	100.01
Si	3.05	3.04	3.05	3.05	3.04	3.05
Al	0.95	0.95	0.95	0.95	0.96	0.95
Ca	0.00	0.00	0.00	0.00	0.00	0.00
Na	0.03	0.03	0.02	0.02	0.03	0.03
K	0.94	0.94	0.93	0.92	0.93	0.94
Ba	0.00	0.00	0.00	0.00	0.00	0.00
An	0.00	0.51	0.41	0.00	0.10	0.00
Ab	3.22	3.04	2.52	2.01	2.81	2.59
Or	96.78	96.45	97.07	97.99	97.09	97.41

(data from Liu (2010))

muscovite (193.6 ± 6 Ma) intergrown with the dated cassiterite sample that yielded an inverse isochron age of 194.53 ± 1.0 Ma (Zhang et al., 2014); and (6) an $^{40}Ar/^{39}Ar$ inverse isochron age for muscovite associated with coarse-grained beryl from Zone III (see below for the zone definitions) of 195.7 ± 2.5 Ma (Liu, 2017). All these age data indicates that mineralization was coeval with the Pankou and Pukouling granites (Figs. 2–3). The contents of Be, W, Sn, Li, Cs, and Rb in the Pankou and Pukouling granites (Ye et al., 2001; Cao et al., 2004; Liu et al., 2012a) are high (Wedepohl, 1995; Hu and Gao, 2008), and consistent with contents of these elements in other W–Sn-bearing granites (Wu et al., 2017; Mao et al., 2019).

The main mineralization in the Xuebaoding deposit occurs in extensional joints in white marble and schist near the margins of the Pankou and Pukouling granites, and only minor fine-grained beryl and cassiterite occur in the granites (Fig. 3 of Liu et al., 2012).

As has been reported, three zones in ore veins could be recognized according to the wallrock and mineral assemblages (Liu et al., 2012a) as fellows: The ore veins can be broadly divided into three zones, based on mineralogy and host rock type (Fig. 3). Zone I is in the granite and dominated by muscovite and beryl; Zone II is located at the transition from granite to marble and consists mainly of beryl, cassiterite, and muscovite. This is consistent with the division of the granites into central and border facies based on decreasing grain size (Fig. 1); Zone III contains the main mineralization and is hosted by marble and schist, which contains beryl, cassiterite, scheelite, fluorite, calcite, and acicular tourmaline. The veins have a center that consists of monomineralic quartz, and a margin that consists of coarse-grained beryl, cassiterite, scheelite, feldspar, albite, muscovite, fluorite, and apatite (Fig. 3). This suggests that the monomineralic vein quartz formed later than the coarse-grained crystals. Muscovite lines the walls of the veins, and beryl, cassiterite, scheelite, fluorite, apatite, K-feldspar, and albite occur as individual crystals or aggregates on muscovite. In general, the Pankou and Pukouling granites exhibit only weak alteration (Fig. 4A–D). Only minor greisen, skarn, and muscovite alteration (up to 0.5 cm thick) was occasionally observed (Fig. 4E–F).

The Pankou and Pukouling alkali granites consist of quartz (35–40 vol%), albite (30–35 vol%), muscovite (30–35 vol%), and minor K-feldspar (0–5 vol%) and mafic minerals. Most main minerals in the granites have diameters of < 100 μm (Fig. 4E). Some albite, muscovite, and K-feldspar are > 600 μm in size and occur as phenocrysts (Fig. 4F). In these granites, albite forms the large and euhedral crystals (Fig. 4G–H) and feldspar is anhedral. Due to the limited exposure of both granites, possible vertical zonation exists like that exhibited by typical Li–F granites (Zhu et al., 2002). Based on thin-section petrography, the Pankou and Pukouling granites can be characterized as albite leucogranites.

Given there are no other veins cutting or overprinting the ore veins, it is inferred that only one stage of fluid activity was involved in the formation of the deposit. In this study, the Pankou and Pukouling granites, selected minerals from the ore veins, and marble samples were chosen for analysis. The detailed analytical methods are described in the Supplementary Material.

3. Results

3.1. Mineral chemistry

In the Xuebaoding deposit, albite is one of the main rock-forming minerals along with quartz and muscovite in Pankou and Pukouling granites. The albite is very pure and has a high Ab content (96.78–99.52 mol.%), low An (0.00–2.42 mol.%) and Or (0.06–0.95 mol.%) contents (Table 1). Alkali feldspar occurs as small crystals or relicts in albite in the leucogranites and has high Or contents (96.45–97.99 mol.%), low Ab (2.01–3.22 mol.%) and An (0.00–0.51 mol.%) contents (Table 2). Muscovite in the leucogranites is pure and only contains trace amounts of FeO (0.32–2.80 wt%) and TiO_2 (0.00–0.81 wt%) (Table 3).

3.2. Marble geochemistry

The white marble has variable contents of W (0.20–2.37 ppm; average = 0.97 ppm), Sn (0.23–0.82 ppm; average = 0.34 ppm), Be (0.05–0.21 ppm; average = 0.14 ppm), Li (3.15–10.5 ppm; average = 6.02 ppm), Rb (0.30–2.74 ppm; average = 0.94 ppm), and Cs (0.06–0.91 ppm; average = 0.38 ppm (Table 4). These results suggest that the marble is relatively pure. The 6 analyzed marble samples have similar primitive-mantle-normalized trace element patterns (Fig. 5), and low rare earth element (REE) contents, which are consistent with previous analyses of the marble (Liu et al., 2012a). The trace element patterns exhibit negative anomalies for Nb, Ce, Nd, Zr, and Yb, and positive anomalies for U, Sr, Pb, Y, Lu, and Tm. The chondrite-normalized REE patterns are characterized by slight negative Eu anomalies and light REE enrichments.

Table 3
EMPA results of muscovite as rock-forming mineral in Pankou granites, Xuebaoding deposit.

Samples	Mus 4–1-1	Mus 4–1-2	Mus 4–1-3	Mus 4–1-4	Mus 4–2-1	Mus 4–2-2	Mus 4–2-3	Mus 4–2-4	Mus 4–3-1	Mus 4–3-2	Mus 4–3-3	Mus 4–3-4
Na_2O	0.42	0.27	0.17	0.29	0.35	0.27	0.30	0.31	0.47	0.27	0.23	0.33
MgO	1.31	1.65	0.62	1.60	0.42	0.80	2.37	0.56	0.35	0.23	0.18	1.12
Al_2O_3	32.44	32.22	32.23	31.25	34.30	33.97	30.00	34.78	34.83	34.90	35.15	32.75
SiO_2	49.48	49.48	53.73	49.59	49.50	49.61	50.14	49.81	49.35	49.86	50.37	50.37
K_2O	11.01	10.82	10.86	10.86	11.03	11.16	10.62	11.10	10.87	10.72	10.51	10.23
CaO	0.00	0.08	0.00	0.12	0.00	0.05	0.01	0.00	0.11	0.06	0.02	0.09
TiO_2	0.43	0.40	0.00	0.57	0.13	0.53	0.81	0.01	0.14	0.06	0.06	0.28
V_2O_5	0.21	0.11	0.13	0.10	0.00	0.00	0.14	0.02	0.00	0.00	0.00	0.00
Cr_2O_3	0.00	0.02	0.14	0.02	0.17	0.00	0.07	0.03	0.08	0.09	0.02	0.11
MnO	0.00	0.24	0.00	0.36	0.00	0.29	0.13	0.13	0.11	0.08	0.21	0.28
FeO	2.80	1.94	0.32	1.58	1.64	1.68	1.74	1.71	2.04	2.32	2.02	2.02
CoO	0.20	0.05	0.02	0.10	0.07	0.02	0.00	0.04	0.00	0.00	0.00	0.00
Total	98.30	97.28	98.22	96.44	97.61	98.38	96.33	98.50	98.35	98.59	98.77	97.58
Si	3.23	3.24	3.42	3.27	3.22	3.20	3.31	3.21	3.19	3.21	3.22	3.27
Al^{IV}	0.77	0.76	0.58	0.73	0.78	0.80	0.69	0.79	0.81	0.79	0.78	0.73
Al^{VI}	1.72	1.72	1.84	1.70	1.85	1.79	1.64	1.85	1.84	1.85	1.87	1.77
Ti	0.02	0.02	0.00	0.03	0.01	0.03	0.04	0.00	0.01	0.00	0.00	0.01
Fe^{3+}	0.15	0.11	0.02	0.09	0.09	0.09	0.10	0.09	0.11	0.12	0.11	0.11
Fe^{2+}	0.00	0.00	0.00	0.00	0.00	0.00	0.00	0.00	0.00	0.00	0.00	0.00
Mn	0.00	0.01	0.00	0.02	0.00	0.02	0.01	0.01	0.01	0.00	0.01	0.02
Mg	0.13	0.16	0.06	0.16	0.04	0.08	0.23	0.05	0.03	0.02	0.02	0.11
Ca	0.00	0.01	0.00	0.01	0.00	0.00	0.00	0.00	0.01	0.00	0.00	0.01
Na	0.05	0.03	0.02	0.04	0.04	0.03	0.04	0.04	0.06	0.03	0.03	0.04
K	0.92	0.90	0.88	0.91	0.91	0.92	0.89	0.91	0.90	0.88	0.86	0.85
Total	6.99	6.97	6.82	6.96	6.94	6.95	6.95	6.95	6.96	6.92	6.90	6.91
OH^-	2.00	2.00	2.00	2.00	2.00	2.00	2.00	2.00	2.00	2.00	2.00	2.00
MF	0.45	0.57	0.78	0.59	0.31	0.42	0.69	0.35	0.22	0.15	0.13	0.46
$Al^{VI} + Fe^{3+} + Ti$	1.89	1.85	1.86	1.82	1.94	1.91	1.78	1.94	1.96	1.98	1.98	1.89
$Fe^{2+} + Mn$	0.00	0.01	0.00	0.02	0.00	0.02	0.01	0.01	0.01	0.00	0.01	0.02
Ti/(Mg + Fe + Ti + Mn)	0.07	0.07	0.00	0.10	0.05	0.12	0.11	0.00	0.04	0.02	0.02	0.06
Al/(Al + Mg + Fe + Ti + Mn + Si)	0.41	0.41	0.41	0.40	0.44	0.43	0.39	0.44	0.44	0.44	0.44	0.42
XFe	0.68	0.54	0.34	0.50	0.80	0.68	0.42	0.75	0.85	0.91	0.92	0.64

(data from Liu (2010))

3.3. Geochemistry of the Pankou and Pukouling granites

Twenty-one granites were analyzed for major and trace elements. The loss-on-ignition (LOI) values range from 0.64 to 5.33 wt%. Both granites have variable SiO_2 contents of 59.18–74.91 wt%, high alkali contents, with Na_2O (3.45–9.11 wt%) being higher than K_2O (2.68–6.56 wt%) (Table 5). These granitic rocks plot in or above the high-K field in a K_2O vs. SiO_2 diagram (Fig. 6A). In a (Na_2O + K_2O) vs. SiO_2 diagram (Fig. 6B), the samples plot in the syenite field rather than the granite field due to the high alkali and low SiO_2 contents. However, there is no arfvedsonite or aegirine–augite in the granites, suggesting the samples are not syenites (Liu and Hou, 2017; Liu et al., 2019a; 2019b). Given that muscovite, albite, feldspar, and quartz are the main rock-forming minerals, the samples can still be characterized as a type of granite. In Fig. 6B–C, the chemical trends of these samples do not follow those of I-type granites. The granites are clearly peraluminous, with alumina saturation index (A/CNK) values of 1.09–1.63 (Fig. 6D). P_2O_5, MgO, TiO_2, and TFe_2O_3 contents are 0.01–0.15, 0.01–0.53, 0.01–0.17, and 0.17–0.76 wt%, respectively. The high-field-strength elements contents are low. For example, Zr and Hf contents are 13.6–41.6 and 1.32–4.34 ppm, respectively. The granites also have low REE contents of 0.2–11.0 ppm (Table 5). The samples are relatively enriched in Rb, Ta, Sr, P, and Pb, and depleted in Ba, La, Ce, and Nd (Fig. 7A). Whole-rock chondrite-normalized REE patterns of all samples are characterized by negative Eu anomalies (0.01–0.17), moderate light REE enrichment with La/Yb_N = 1.13–6.07, except for two samples with 0.55–0.73, and nearly flat heavy REE patterns (Fig. 7B). Apart from sample PK-6, 20 samples have similar trace element patterns with slight light REE enrichment. Five samples (PK-3, PK-4, PK-5, PK-17, and PK-30) exhibit Eu enrichment, and the other samples exhibit Eu depletion.

The Pankou and Pukouling granites are characterized by: (1) low transition metal contents, with Sc = 0.62–3.50 and 0.79–3.97 ppm, Ti = 0.01–0.06 and 0.04–0.17 wt%, V = 1.55–8.39 and 0.57–5.38 ppm, Cr = 30.3–173 and 12.1–14.2 ppm, Mn = 0.01–0.05 and 0.06–0.08 wt%, Fe = 0.22–0.76 and 0.17–0.71 wt%, Co = 0.02–1.04 and 0.53–1.62 ppm, Ni = 5.21–25.5 and 0.47–2.00 ppm, respectively; (2) enrichments of volatile elements and rare-metal elements, with Li = 149–624 and 169–846 ppm, Be = 6.73–1681 and 21.1–49.5 ppm, B = 30.3–465 ppm and below detection, W = 5.94–54.1 and 2.07–18.5 ppm, Sn = 28.9–200 and 41.3–120 ppm, Cs = 36.2–204 and 49.3–212 ppm, Rb = 275–548 and 370–618 ppm, F = 0.04–0.21 wt% and below detection, respectively. The contents of B, F, and rare-metal elements are significantly high (Table 5).

The relatively high REE contents indicate that both granites were the main source of the mineralization, given the low REE and trace element contents of the marble samples (Liu et al., 2012a; Table 4-5).

3.4. Sr–Nd–Pb isotopes

Sr–Nd–Pb isotope ratios of the granite samples are listed in Tables 6 and 7. The granite samples have $(^{87}Sr/^{86}Sr)_i$ = 0.673054–0.732583 and $^{143}Nd/^{144}Nd$ = 0.511175–0.511966, with $\varepsilon_{Nd}(t)$ values of − 11.49 to − 23.19. Due to the low $\varepsilon_{Nd}(t)$ values, calculated two-stage model ages are reliable. Lead isotope ratios of the granite samples are $^{206}Pb/^{204}Pb$ = 18.710–19.908, $^{207}Pb/^{204}Pb$ = 15.647–15.730, and $^{208}Pb/^{204}Pb$ = 38.434–38.929 (Fig. 8).

3.5. Boron isotopic composition of tourmaline

In situ B isotope data are listed in Table 8. The three types of tourmaline have similar $\delta^{11}B$ values (−11.21‰ to − 13.65‰; Table 8), indicating a similar source for their corresponding fluids. The type II tourmaline collected from the border of the granites has $\delta^{11}B$ = − 11.21‰ to − 12.40‰. Type I and III tourmalines have similar $\delta^{11}B$

Table 4
Trace elements of host marble in Xuebaoding, Sichuan Province (ppm).

Samples	XD 11	XD 12	XD 13	XD 14	XD 16	XD 17	XD 20
Y	3.94	4.07	3.13	2.66	2.96	4.05	4.61
La	2.00	1.58	1.27	1.13	1.47	1.85	2.24
Ce	0.86	0.89	0.80	0.57	0.85	1.40	1.62
Pr	0.33	0.27	0.22	0.18	0.22	0.30	0.40
Nd	1.46	1.12	0.93	0.84	0.99	1.24	1.73
Sm	0.27	0.22	0.18	0.16	0.18	0.23	0.38
Eu	0.06	0.07	<0.05	<0.05	<0.05	0.07	0.07
Gd	0.36	0.35	0.22	0.18	0.25	0.30	0.39
Tb	0.05	0.05	<0.05	<0.05	<0.05	0.05	0.07
Dy	0.34	0.35	0.23	0.19	0.21	0.36	0.41
Ho	0.08	0.08	0.06	<0.05	0.05	0.08	0.09
Er	0.20	0.22	0.16	0.14	0.14	0.22	0.28
Tm	<0.05	<0.05	<0.05	<0.05	<0.05	<0.05	<0.05
Yb	0.17	0.16	0.14	0.13	0.11	0.23	0.22
Lu	<0.05	<0.05	<0.05	<0.05	<0.05	<0.05	<0.05
Li	7.35	4.16	4.20	6.75	3.15	10.5	18.2
Be	0.21	0.05	0.16	0.16	0.09	0.19	0.13
Sc	1.53	1.66	1.56	1.38	1.35	1.75	1.69
V	0.08	0.10	0.08	<0.05	0.04	0.07	0.98
Cr	4.01	3.81	3.82	3.63	4.85	3.53	4.67
Ni	31.6	32.3	31.4	29.9	30.2	31.4	31.0
Cu	5.31	3.44	4.03	4.51	3.52	4.66	4.58
Zn	9.06	7.58	6.13	6.39	5.57	7.61	6.89
Ga	0.09	0.10	0.08	0.07	0.07	0.25	0.18
Rb	0.30	0.31	0.49	0.47	1.35	2.74	3.76
Sr	194	209	202	194	208	247	168
Zr	0.55	0.50	0.61	0.50	0.40	1.73	1.86
Nb	0.05	<0.05	0.05	<0.05	<0.05	0.14	0.17
Mo	<0.05	0.06	<0.05	<0.05	<0.05	0.07	0.06
Cd	0.28	0.24	0.27	0.38	0.17	0.33	0.41
In	<0.05	<0.05	<0.05	<0.05	<0.05	<0.05	<0.05
Sn	0.24	0.27	0.23	0.25	0.23	0.82	0.33
Sb	0.06	0.09	0.06	<0.05	0.10	0.08	0.07
Cs	0.12	0.38	0.31	0.50	0.06	0.91	0.29
Ba	6.71	6.10	4.52	3.14	3.99	5.01	4.54
Hf	<0.05	<0.05	<0.05	<0.05	<0.05	0.06	0.05
Ta	<0.05	<0.05	<0.05	<0.05	<0.05	<0.05	<0.05
W	0.36	0.20	0.61	2.37	0.38	1.89	15.3
Tl	<0.05	<0.05	<0.05	<0.05	<0.05	<0.05	<0.05
Pb	0.50	0.91	0.87	0.44	0.32	1.11	0.53
Bi	<0.05	<0.05	<0.05	<0.05	<0.05	<0.05	0.05
Th	0.06	0.07	0.09	0.07	0.05	0.20	0.13
U	0.06	<0.05	0.06	<0.05	0.13	0.07	0.16

Data from Liu (2010).

values of − 11.88‰ to − 13.65‰ and − 12.13‰ to − 13.24‰, respectively, which are slightly lighter than the type II tourmaline. In addition, the tourmaline crystals do not show significant core-to-rim B isotopic variations.

4. Discussion

4.1. Petrogenesis of the Pankou and Pukouling granites

Based on geochemical and mineralogical criteria, granitoid rocks have traditionally been classified as I-, S-, and A-type (Chappell and White, 1974, 1992; Hineab et al., 1978; Whalen et al., 1987). A-type granitoids typically contain high-temperature anhydrous minerals, such as pyroxene, fayalite, and interstitial biotite (Collins et al., 1982; Whalen et al., 1987; Eby, 1992), and are characterized by high FeOT/MgO ratios, enrichment of high-field-strength elements and REEs, Zr concentrations of > 250 ppm, and Zr + Nb + Ce + Y contents of > 350 ppm (Eby, 1990, 1992; Frost and Frost, 2011). The Pankou and Pukouling granites have low FeOT/MgO ratios and Zr and Zr + Nb + Ce + Y contents, and contain no high-temperature anhydrous minerals. Thus, the Pankou and Pukouling granites are not A-type granites. I-type granites contain hornblende (Chappell and White, 1992, 2001; Roberts and Clemens, 1993), and are metaluminous to weakly peraluminous, with A/CNK < 1.1 (Chappell and White, 1992; Chappell, 1999). In contrast, S-type granites are strongly peraluminous magmas formed mostly from metasedimentary rocks, and typically contain abundant inherited zircons (Collins and Richards, 2008) and Al-rich minerals, such as muscovite, garnet, and cordierite, and are always strongly peraluminous with high A/CNK (>1.1; Chappell and White, 1992; Chappell, 1999; Clemens, 2003). Our samples have high A/CNK ratios (1.09–1.63). No hornblende, but abundant muscovite and tourmaline, are present in the studied samples. The negative correlation between P_2O_5 and SiO_2 is a key criterion used to distinguish I-type from S-type granites (Chappell and White, 1992). The studied samples show no significant negative correlation between P_2O_5 and SiO_2 (Fig. 6C). Thus, as S-type granites are generally derived from metasedimentary rocks, the Pankou and Pukouling albite granites are typical S-type granitoids, and were likely derived by partial melting of metasedimentary rocks. Their similar Sr–Nd–Pb isotopic compositions indicate a similar origin for the Pankou and Pukouling albite granites (Fig. 8).

Previous studies (Morgan et al., 1990; London, 1992; Dingwell et al., 1996; Hervig et al., 2002; Thomas et al., 2003; Tonarini et al., 2003; Wunder et al., 2005; Trumbull et al., 2008) have shown that natural melts rich in B, F, Li, and H_2O could crystallize tourmaline more readily (i.e., tetrahedral but not trigonal boron complexes). Three types of tourmaline in Xuebaoding could be found. The partitioning of ^{11}B and ^{10}B between borosilicate, melt, and/or fluid depends on the coordination environment of B in these phases and the isotopic fractionation factor is also temperature and pressure dependent (Palmer et al., 1992; Palmer and Swihart, 1996; Williams et al., 2001; Hervig et al., 2002; Wunder et al., 2005; Trumbull et al., 2008). During fractionation between tourmaline and fluid, the former is always enriched in ^{10}B, while ^{11}B is preferentially retained in the fluid (Palmer et al., 1992).

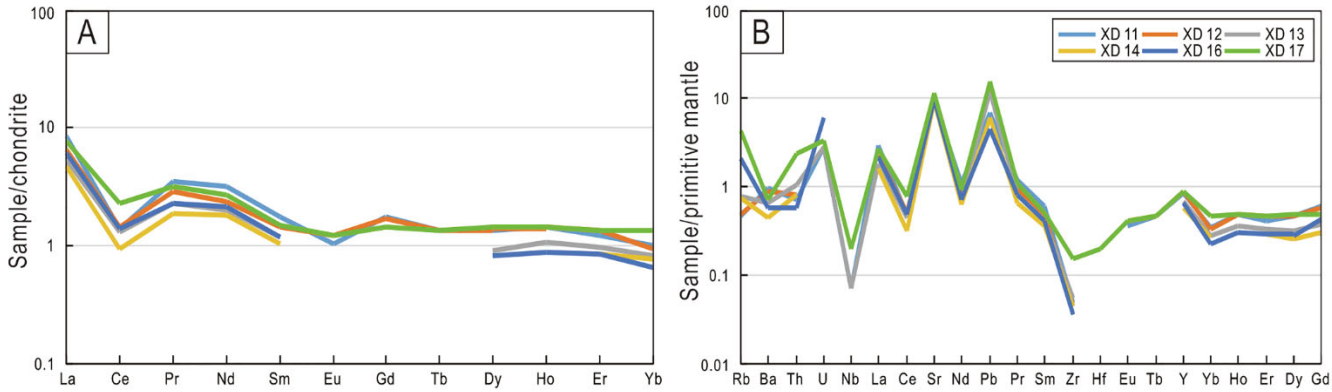

Fig. 5. (A) Chondrite-normalized REE and (B) primitive-mantle-normalized trace element patterns of the marble. The primitive mantle normalizing values were taken from McDonough and Sun (1995).

Table 5
Major and trace elements of the Pankou and Pukouling granites in Xuebaoding deposit, Sichuan Province.

Sample	*PK − 1(Pankou)*	*PK − 2(Pankou)*	*PK − 3(Pankou)*	*PK − 4(Pankou)*	*PK − 5(Pankou)*	*PK − 6(Pankou)*	*PK − 7(Pankou)*	*PK − 8(Pankou)*	*PK − 9(Pankou)*	*PK − 10(Pankou)*	*PK − 11(Pankou)*	*PK − 14(Pankou)*	*PK − 17(Pankou)*	*PK − 23(Pankou)*	*PK − 30(Pankou)*	*PK − 33(Pankou)*	*PK − 34(Pankou)*	*PANK2(Pukouling)*	*PANK5(Pukouling)*	*PKZW1(Pukouling)*	*PKZW2(Pukouling)*
Wt%																					
SiO_2	63.16	69.65	60.20	59.50	64.94	62.17	63.46	64.60	61.96	64.15	65.00	67.64	59.18	61.29	62.60	63.52	64.28	68.51	74.91	68.31	73.58
TiO_2	0.03	0.04	0.06	0.06	0.01	0.02	0.03	0.02	0.05	0.03	0.02	0.02	0.04	0.04	0.04	0.03	0.03	0.17	0.04	0.07	0.15
Al_2O_3	21.92	14.90	24.78	23.77	20.29	22.05	21.78	20.47	22.36	22.01	20.51	18.89	25.39	24.07	22.78	21.75	21.40	18.45	14.90	18.19	15.62
TFe_2O_3	0.38	0.73	0.60	0.65	0.24	0.40	0.33	0.22	0.76	0.33	0.46	0.45	0.63	0.44	0.41	0.37	0.36	0.67	0.21	0.17	0.71
FeO	0.33	0.39	0.37	0.58	0.21	0.21	0.26	0.18	0.39	0.33	0.46	0.44	0.76	0.48	0.56	0.28	0.46	1.41	0.68	1.04	1.20
MnO	0.03	0.03	0.04	0.05	0.01	0.03	0.02	0.02	0.03	0.02	0.02	0.02	0.02	0.03	0.02	0.02	0.02	0.07	0.06	0.08	0.06
MgO	0.09	0.13	0.15	0.25	0.01	0.12	0.11	0.05	0.17	0.07	0.07	0.08	0.27	0.14	0.10	0.08	0.08	0.53	0.17	0.26	0.46
CaO	0.38	0.32	0.17	0.18	0.17	0.28	0.34	0.33	0.20	0.25	0.16	0.14	0.29	0.11	0.24	0.35	0.23	0.32	0.59	0.53	0.58
Na_2O	7.51	5.12	6.82	6.89	6.94	7.02	7.88	7.15	6.36	9.11	7.05	6.31	5.61	5.93	7.87	7.70	8.59	3.45	4.48	4.94	3.92
K_2O	4.74	3.26	4.72	4.22	5.88	5.44	4.45	5.86	5.87	2.68	5.69	4.73	6.56	6.16	4.10	4.62	3.39	4.71	3.73	3.61	4.69
P_2O_5	0.15	0.11	0.02	0.01	0.04	0.10	0.08	0.12	0.11	0.05	0.07	0.03	0.01	0.02	0.02	0.15	0.08	0.11	0.14	0.13	0.11
F(%)	0.15	0.14	0.16	0.21	0.04	0.15	0.14	0.13	0.18	0.13	0.09	0.10	0.18	0.17	0.14	0.13	0.11	–	–	–	–
LOI	1.12	5.33	2.32	3.96	0.84	2.16	0.98	0.68	1.94	1.18	0.82	1.18	2.04	1.78	1.52	1.28	0.86	1.75	0.64	0.93	2.06
$Na_2O + K_2O$	12.25	8.38	11.54	11.11	12.82	12.46	12.33	13.01	12.23	11.79	12.74	11.04	12.17	12.09	11.97	12.32	11.98	8.16	8.21	8.55	8.61
A/CNK	1.2						1	1	1	1	1	1	0	1	1	1	1		1	1	1
Total	99.66	99.76	100	99.75	99.41	99.94	99.6	99.65	99.99	100	99.96	99.59	100	100	99.84	100	99.43	98.74	99.87	97.22	102
ppm																					
La	0.74	2.80	0.12	0.08	0.12	0.40	0.45	0.70	0.38	0.28	0.26	0.21	0.04	0.55	0.09	0.57	0.60	6.29	2.42	7.48	3.50
Ce	1.60	5.31	0.18	0.14	0.24	0.84	1.07	1.47	0.82	0.55	0.60	0.49	0.08	0.93	0.15	1.25	1.28	9.15	4.34	12.5	7.66
Pr	0.21	0.61	0.02	0.01	0.04	0.12	0.15	0.19	0.13	0.07	0.09	0.05	0.01	0.12	0.02	0.17	0.17	1.38	0.57	1.66	0.75
Nd	0.82	2.24	0.11	0.04	0.16	0.53	0.66	0.82	0.60	0.36	0.36	0.23	0.07	0.47	0.09	0.63	0.70	4.64	2.13	6.00	2.33
Sm	0.24	0.63	0.04	0.01	0.05	0.18	0.22	0.26	0.17	0.1	0.11	0.07	0.02	0.11	0.03	0.17	0.20	1.29	0.76	1.59	0.81
Eu	0.03	0.04	0.02	0.01	0.02	0.01	0.03	0.05	0.03	0.02	0.02	0.02	0.04	0.02	0.02	0.03	0.02	0.09	0.17	0.13	0.05
Gd	0.32	0.65	0.05	0.01	0.06	0.25	0.28	0.30	0.26	0.12	0.14	0.09	0.03	0.11	0.04	0.26	0.27	1.38	1.27	1.58	0.68
Tb	0.06	0.14	0.01	0.00	0.01	0.05	0.06	0.06	0.06	0.02	0.03	0.02	0.01	0.02	0.01	0.06	0.06	0.29	0.32	0.29	0.16
Dy	0.38	0.87	0.06	0.02	0.07	0.32	0.40	0.42	0.39	0.15	0.22	0.11	0.04	0.12	0.05	0.41	0.41	1.71	1.92	1.70	0.89
Ho	0.07	0.15	0.01	0.01	0.02	0.05	0.07	0.08	0.08	0.03	0.04	0.02	0.01	0.02	0.01	0.07	0.07	0.30	0.28	0.29	0.13
Er	0.18	0.37	0.04	0.02	0.05	0.13	0.16	0.19	0.21	0.07	0.11	0.05	0.03	0.06	0.04	0.16	0.17	0.78	0.62	0.74	0.32
Tm	0.03	0.05	0.01	0.00	0.01	0.02	0.02	0.03	0.03	0.01	0.02	0.01	0.01	0.01	0.01	0.02	0.03	0.11	0.08	0.10	0.05
Yb	0.16	0.31	0.05	0.03	0.06	0.10	0.14	0.17	0.22	0.08	0.11	0.05	0.05	0.07	0.08	0.13	0.16	0.70	0.47	0.62	0.32
Lu	0.02	0.04	0.01	0.01	0.01	0.02	0.02	0.03	0.04	0.01	0.02	0.01	0.01	0.01	0.02	0.02	0.03	0.09	0.07	0.08	0.05
Hf	2.97	2.29	1.95	2.49	2.61	2.18	2.24	2.03	2.96	3.05	1.70	1.32	4.16	3.10	4.34	2.63	2.70	1.88	1.43	1.72	1.56
Ta	14.6	21.7	8.17	11.9	1.01	8.57	5.33	7.77	4.46	6.66	4.84	6.10	13.8	8.85	7.18	16.3	4.96	15.5	7.32	10.2	8.12
Y	2.57	4.06	0.42	0.20	0.42	1.72	2.00	2.29	1.97	0.84	1.06	0.52	0.24	0.47	0.35	1.85	2.02	8.40	8.70	8.36	4.13
Li	178	273	427	624	159	243	230	167	287	197	149	229	345	373	270	165	203	846	238	606	169
Be	89.8	93.5	1166	1681	859	73.2	169	6.73	29.1	138	151	408	32.5	487	181	131	147	22.0	21.1	23.1	49.5
Sc	2.48	1.00	3.16	3.50	1.67	3.42	1.81	0.79	2.38	0.97	1.67	1.45	0.62	1.77	1.22	1.06	0.82	3.97	0.91	3.65	0.79
V	4.95	2.11	7.38	6.34	5.92	2.88	6.22	5.33	6.12	4.75	5.63	4.10	4.80	8.39	5.63	5.56	1.55	5.38	0.87	4.93	0.57
Cr	30.3	127	47.6	63.1	69.1	43.2	36.2	60.4	49.7	173	67.7	131	31.8	125	55.0	51.3	98.9	13.4	14.2	12.3	12.1
Ni	25.5	5.62	13.4	15.6	14.7	22.5	19.4	6.43	11.5	5.21	8.91	8.96	7.88	25.5	7.34	5.60	7.67	2.00	0.95	1.44	0.47
Cu	6.71	9.19	5.29	5.77	2.06	9.82	5.36	5.53	18.3	2.25	6.51	4.53	3.35	5.74	2.31	4.45	5.01	4.78	5.87	7.32	27.7
Zn	24.5	43.9	37.7	35.4	11.2	29.1	21.2	17.5	50.3	30.9	16.6	19.0	23.7	33.5	10.5	28.6	17.6	78.1	37.5	96.6	46.7
Ga	44.9	23.6	64.1	65.9	25.7	47.8	43.7	34.9	42.0	33.1	31.8	33.1	34.7	51.1	45.1	40.6	41.5	41.4	21.1	37.2	30.3
Rb	493	338	548	478	464	543	444	508	466	275	450	396	478	543	388	431	292	618	370	489	415
Sr	130	53.4	54.8	62.9	103	94.1	104	160	76.1	60.8	88.9	54.6	210	62.1	79.6	135	59.4	11.7	30.9	16.6	30.7
Zr	38.7	30.2	27.3	30.2	26.2	28.3	21.8	25.5	41.2	27.1	18.8	13.6	36.9	29.7	41.6	26.3	30.7	36.5	23.8	30.8	14.7
Nb	24.5	31.1	34.1	40.7	4.95	29.0	23.1	15.9	22.1	16.1	15.9	15.5	23.7	26.7	21.9	23.8	16.1	52.1	17.3	36.6	28.4

(*continued on next page*)

Table 5 (*continued*)

Sample	PK − 1(Pankou)	PK − 2(Pankou)	PK − 3(Pankou)	PK − 4(Pankou)	PK − 5(Pankou)	PK − 6(Pankou)	PK − 7(Pankou)	PK − 8(Pankou)	PK − 9(Pankou)	PK − 10(Pankou)	PK − 11(Pankou)	PK − 14(Pankou)	PK − 17(Pankou)	PK − 23(Pankou)	PK − 30(Pankou)	PK − 33(Pankou)	PK − 34(Pankou)	PANK2(Pukouling)	PANK5(Pukouling)	PKZW1(Pukouling)	PKZW2(Pukouling)
Mo	0.59	1.75	0.79	1.21	1.09	0.68	0.56	0.99	0.76	2.40	1.10	1.77	0.48	2.11	2.08	0.90	1.46	<0.05	<0.05	<0.05	<0.05
Cd	0.26	0.24	0.53	0.52	0.11	0.27	0.20	0.16	0.35	0.57	0.16	0.22	0.48	0.20	0.37	0.26	0.17	0.10	<0.05	<0.05	0.16
In	<0.05	<0.05	0.06	0.06	<0.05	<0.05	<0.05	<0.05	<0.05	0.06	<0.05	<0.05	<0.05	<0.05	<0.05	<0.05	<0.05	<0.05	<0.05	<0.05	<0.05
Sn	77.8	44.3	148	154	28.9	79.8	63.5	44.5	99.3	200	53.8	50.4	141	101	121	72.9	52.1	120	41.3	113	77.4
Sb	1.00	0.07	0.61	1.06	0.20	0.89	0.10	2.19	8.49	0.74	1.30	2.41	<0.05	1.56	0.74	1.76	2.38	0.96	0.12	1.31	7.19
Cs	65.8	57.1	156	204	104	61.8	60.1	61.9	46.4	36.2	56.6	69.3	100	92.6	52.4	62.9	46.8	212	65.6	110	49.3
Ba	20.6	20.6	34.9	10.6	33.0	21.5	27.2	85.3	45.1	16.3	34.3	31.7	203	28.9	22.0	20.2	21.3	63.4	42.7	69.5	9.26
W	7.22	30.3	7.4	11.4	6.56	23.2	5.94	6.37	54.1	7.32	7.49	11.2	9.47	6.68	11.6	9.86	6.75	7.79	2.07	18.5	3.12
Tl	3.13	2.39	3.02	2.83	3.61	3.55	2.80	3.65	3.24	1.67	3.42	3.03	3.56	3.78	2.37	3.01	2.12	3.24	2.04	2.61	2.17
Pb	20.4	44.6	8.55	12.8	17.0	18.0	12.8	24.4	20.3	8.32	22.0	19.0	17.6	11.9	20.5	27.6	30.4	13.0	46.8	39.1	35.5
Bi	0.94	3.10	0.17	0.90	0.62	0.91	0.14	0.77	1.35	0.14	0.77	1.23	0.05	0.33	0.88	1.69	0.72	3.42	0.56	6.49	2.05
Th	1.06	2.27	4.29	0.31	0.53	2.12	0.67	0.79	1.60	1.32	0.43	0.74	0.91	0.82	0.63	0.87	1.43	2.09	1.64	3.05	1.67
U	10.1	12.4	5.31	6.11	3.02	4.81	5.29	7.25	6.06	6.71	2.13	5.31	3.69	7.08	5.92	9.55	5.94	2.85	4.89	14.6	8.74
Co	0.03	1.04	0.08	0.1	0.63	0.02	0.41	0.39	0.67	0.45	0.59	0.74	0.55	0.59	0.54	0.47	0.42	1.51	0.60	1.62	0.53
B	65.7	465	106	112	33.2	67.4	52.9	30.3	75.8	65.1	38.1	51.3	124	127	80.3	59.4	51.2	–	–	–	–
Zr/Hf	13.0	13.2	14.0	12.1	10.0	13.0	9.70	12.6	13.9	8.87	11.1	10.3	8.87	9.58	9.59	10.0	11.4	19.4	16.6	17.9	9.42
Nb/Ta	1.68	1.44	4.17	3.43	4.90	3.39	4.34	2.04	4.95	2.42	3.28	2.54	1.71	3.02	3.05	1.46	3.25	3.36	2.36	3.59	3.50
∑REE	9.91	19.3	4.31	4.09	3.01	8.16	7.54	7.85	7.77	3.68	4.86	3.40	1.31	4.86	2.23	6.86	7.01	40.6	25.0	46.77	22.62
δEu	0.33	0.19	1.37	3.02	1.11	0.14	0.37	0.55	0.44	0.56	0.49	0.77	4.98	0.55	1.77	0.44	0.26	0.20	0.53	0.25	0.20
Gd/Yb	2.00	2.10	1.00	0.33	1.00	2.50	2.00	1.76	1.18	1.50	1.27	1.80	0.60	1.57	0.50	2.00	1.69	1.97	2.70	2.55	2.13
La/Sm	3.08	4.44	3.00	8.00	2.40	2.22	2.05	2.69	2.24	2.80	2.36	3.00	2.00	5.00	3.00	3.35	3.00	4.88	3.18	4.70	4.32
La/Yb	4.63	9.03	2.40	2.67	2.00	4.00	3.21	4.12	1.73	3.50	2.36	4.20	0.80	7.86	1.13	4.38	3.75	8.99	5.15	12.1	10.9
La/Nd	0.90	1.25	1.09	2.00	0.75	0.75	0.68	0.85	0.63	0.78	0.72	0.91	0.57	1.17	1.00	0.90	0.86	1.36	1.14	1.25	1.50
Th/U	0.10	0.18	0.81	0.05	0.18	0.44	0.13	0.11	0.26	0.20	0.20	0.14	0.25	0.12	0.11	0.09	0.24	0.73	0.34	0.21	0.10

"–" no determination trace elements of PK samples data from Liu (2010) and other data from this study.

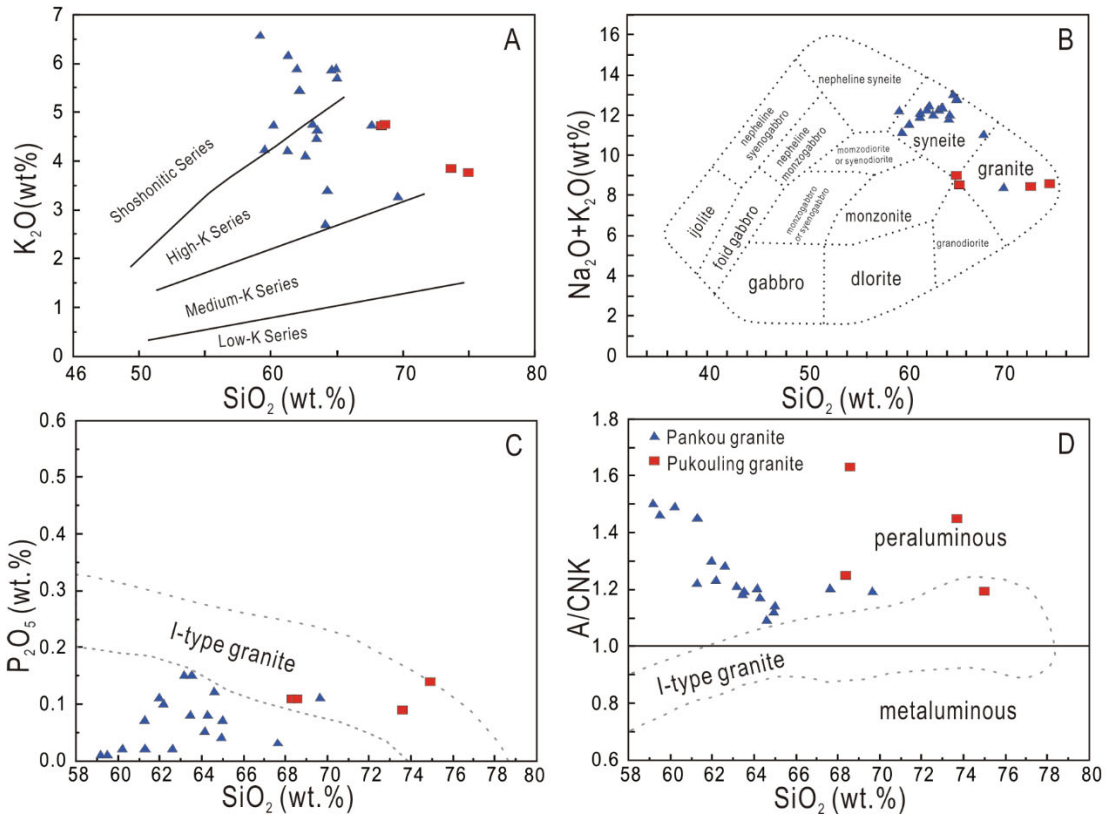

Fig. 6. Plots of (A) K_2O vs. SiO_2 (Gill, 1981), (B) (Na_2O + K_2O) vs. SiO_2 (Middlemost, 1994), (C) P_2O_5 vs. SiO_2, and (D) A/CNK vs. SiO_2 for both Pankou and Pukouling granites. The trends in (C) and (D) for I-type granite are from Chappell (1999).

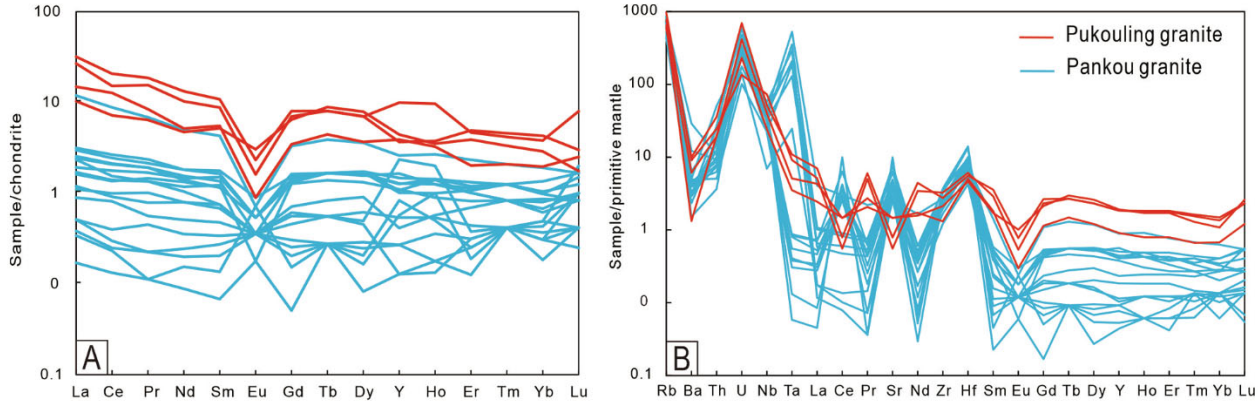

Fig. 7. (A) Chondrite-normalized rare earth element and (B) primitive-mantle-normalized trace element patterns for the Pankou and Pukouling granites.

In this study, B isotope analyses of type I tourmaline ($\delta^{11}B$ = − 11.88‰ to − 13.65‰) formed from an immiscible B-rich aqueous fluid and type III tourmaline (−12.13‰ to − 13.24‰) crystallized directly from magmatic–hydrothermal fluids are slightly lighter than those of type II tourmaline (−11.21‰ to − 12.40‰) originated from granitic melts. Such limited changes in the B isotope values might have been caused by less ^{11}B and ^{10}B fractionation between fluid, melt, and borosilicate. The B isotope values of the three types of tourmaline range from − 11.21‰ to − 13.30‰, and plot in the field for continental crust (Fig. 9), which is also indicative of a metasedimentary source for the host granitic rocks. Based on this, the Sr–Nd–Pb isotope data, and enrichments in Li–F–B–H_2O, the Pankou and Pukouling granites are both S-type granites.

4.2. Enrichment of trace and ore elements

Compared with unfractionated or weakly fractionated granites, K-feldspar in highly fractionated granites is mostly microcline or even amazonite (i.e., Rb-rich K-feldspar), and the amount of plagioclase decreases gradually and evolves towards the Na end-member (Wu et al., 2003a; 2003b). Albite granites are generally regarded as the products of extreme fractionation of granitic magma (Li et al., 2017). In I- and S-type granites, fractionation of amphibole and pyroxene results in Al enrichment and increasing aluminum saturation index values (ASI = Al_2O_3/[CaO + Na_2O + K_2O]), and the formation of muscovite and garnet (i.e., spessartine; Chappell and White, 1992). Rare-metal and volatile element contents of both granites are significantly higher than those of the corresponding Clarke value of crust (Wedepohl, 1995; Hu and Gao, 2008). In addition, volatiles in the residual melts, such as H_2O, Li, F, B, Cl, and

Table 6
Sr and Nd isotope composition of the Pankou and Pukouling granites from Xuebaoding W-Sn-Be deposit Sichuan Province, SW China.

Samples	Rb (ppm)	Sr (ppm)	$^{87}Rb/^{86}Sr$	I_{Sr}	2 s	Sm (ppm)	Nd (ppm)	$^{147}Sm/^{144}Nd$	$(143Nd/144Nd)_i$	$\varepsilon_{Nd}(i)$
PK1(Pankou)	328	138	6.8686	0.720863	0.000011	0.378	0.889	0.2574	0.511615	−13.25
PK2(Pankou)	270	62.5	12.4934	0.727019	0.000014	0.797	2.7	0.1785	0.511708	−13.44
PK3(Pankou)	436	62.6	20.1447	0.732583	0.000013	0.04	0.119	0.2055	0.511175	–23.19
PK4(Pankou)	453	72.4	18.1237	0.721699	0.000016	0.041	0.164	0.1505	0.511502	−18.14
PK5(Pankou)	301	111	7.8444	0.723167	0.00001	0.071	0.207	0.2075	0.511616	−14.49
PK6(Pankou)	354	94.5	10.8594	0.723575	0.000012	0.228	0.441	0.312	0.511373	−16.54
PK7(Pankou)	383	111	10.0011	0.716886	0.000014	0.329	0.751	0.2648	0.511687	−11.65
PK8(Pankou)	396	170	6.7521	0.717571	0.000009	0.324	0.741	0.2642	0.511488	−15.53
PK9(Pankou)	389	82.9	13.5721	0.719711	0.000011	0.313	0.779	0.2432	0.511396	−17.87
PK10(Pankou)	312	74.1	12.1747	0.711569	0.000013	0.148	0.386	0.2317	0.511464	−16.83
PK11(Pankou)	383	105	10.5253	0.718081	0.000013	0.209	0.45	0.2808	0.511464	−15.59
PK14(Pankou)	380	56.3	19.517	0.715097	0.000012	0.08	0.261	0.1849	0.511285	−21.52
PANK2(Pukouling)	618	11.7	159.0742	0.673054	0.000012	1.29	4.64	0.168051	0.511966	−12.39
PANK5(Pukouling)	370	30.9	34.9902	0.709928	0.000009	0.76	2.13	0.215681	0.512030	−12.35
PKZW1(Pukouling)	489	16.6	87.3451	0.712731	0.000009	1.59	6.00	0.160184	0.512002	−11.49

P, tend to increase with crystallization of lepidolite, spodumene, petalite, fluorite, topaz, tourmaline, apatite, and other minerals (i.e., in Li–F granites; Zhu et al., 2002; Wu et al., 2017). The tourmaline usually shows compositional variations from early Mg- and Fe-bearing tourmaline to later Al-bearing elbaite (Zhang et al., 2008). Similarly, mica shows an evolutionary trend from magnesian biotite, magnesian–ferric biotite, and to zinnwaldite and lepidolite (Li and Huang, 2013; Li et al., 2015). Therefore, the presence of elbaite, lepidolite, or Li-bearing muscovite indicates extreme magmatic differentiation of granitic melts. In addition, Wu et al. (2017) noted that most highly fractionated granites are strongly peraluminous. In terms of trace elements, Cr, Ni, Co, Sr, Ba, and Zr tend to decrease, whereas Li, Rb, and Cs become enriched during magmatic differentiation (Gelman et al., 2014; Lee and Morton, 2015). Zr/Hf and Nb/Ta ratios have been used to trace the degree of fractionation of granitic melts (Wu et al., 2017). For example, Zr/Hf = 26 and Nb/Ta ~ 5 reflect the geochemical boundary between highly and extremely fractionated granites (Wu et al., 2017).

The Pankou and Pukouling granites contain most quartz, albite, and muscovite, and the amount of K-feldspar present is low (Fig. 4G–H; Liu et al., 2010). Muscovite and tourmaline occur in the granites. Tourmaline is the main mafic mineral in the Pankou and Pukouling granites, and amphibole and pyroxene are not present. Thus, the Pankou and Pukouling granites can be classified as albite granite. The Pankou and Pukouling granites are strongly peraluminous, with A/CNK > 1.09 (Fig. 10), which is also consistent with these rocks being highly fractionated granites. The studied granites are enriched in Li, Cs, Rb, and ore elements (especially W, Sn, and Be), and depleted in Ni, Sr, Ba, and Zr (Table 5). A large number of apatite, calcite, fluorite, and tourmaline occur in the mineralized veins, indicating enrichment of CO_2, P, F, and B in the granites. The wall-rocks (i.e., marble) are also rich in CO_2. Zr/Hf and Nb/Ta ratios vary from 8.87 to19.4 and from 1.44 to 4.95, respectively, and plot in the extremely fractionated granite field (Fig. 11). In a Zr vs. 10000 × Ga/Al diagram (Fig. 12), the studied granites follow the trend for fractionated I- and S-type granites. Therefore, both granites can be classified as highly fractionated granites. The source of metals during Sn–W mineralization is commonly related to granitic intrusions that are enriched in these metals and volatile elements, such as F, P, Li, and B. The Pankou and Pukouling granites have high concentrations of F (0.04–0.21 wt%) and Li (149–846 ppm), similar with other Li–F granites (Zhu et al., 2002). The studied granites are particularly enriched in Be (21.1–1681 ppm, with an exception of 6.73 ppm) compared with undifferentiated granites (4–6 ppm; London and Evensen, 2002). The presence of beryl in both granites has been attributed to extreme fractional crystallization (Wu et al., 2017). The Pankou and Pukouling granites also have high Sn, Ta, and Li contents (Table 5), and are more enriched in W (2.07–54.1 ppm) than most Li–F granites. For example, W might have been incorporated into muscovite (Cuney et al., 1992). Rare-metal enrichment cannot be solely explained by fractional crystallization and requires a source or accumulation of residual minerals during the evolution of the granitic magma enriched in rare-metals. Highly evolved alkali granites can account for the enrichment of W, Sn, Be, and other ore and trace elements (Raimbault et al., 1995; Lenharo et al., 2002; Esmaeily et al., 2005).

The Pankou and Pukouling granites are not only enriched in W, Sn, and Be, but also alkali elements such as Li, Rb, and Cs, and volatile elements such as B, P, and F, which are essential for concentrating W, Sn and Be (Audétat et al., 2000; Veksler and Thomas, 2002; Breiter et al., 2005). Experimental studies have shown that REEs, F, Li, Rb, Cs, Be, Sn, and W prefer to remain in the melt during fractional crystallization (Keppler and Wyllie, 1991; Linnen, 1998), and the high F content in a H_2O–LiF system increases trace elements solubility of by reducing the viscosity of residual melts and facilitates extreme fractional crystallization (Linnen, 1998; Liu et al., 1999; Audétat et al., 2000; Veksler and Thomas, 2002; Sirbescu and Nabelek, 2003; Duc-Tin et al., 2007). Under these conditions, the exsolution of F-rich fluids in the late magmatic stage would have resulted in high Li, Rb, Cs, W, Sn, and Be concentrations, as described elsewhere in Portugal (Gaans et al., 1995), Brazil (Lenharo et al., 2002), and Iran (Esmaeily et al., 2005). These elements are often enriched near the top of granite bodies (Thomas et al., 2005), which is consistent with the location of the Xuebaoding deposit and limited exposure of the Pankou and Pukouling granites (≤1 km in width and length).

Table 7
Pb isotope composition of the Pankou and Pukouling granite from Xuebaoding W-Sn-Be deposit Sichuan Province, SW China.

sample	U	Pb	Th	$^{206}Pb/^{204}Pb$	±2σ	$^{207}Pb/^{204}Pb$	±2σ	$^{208}Pb/^{204}Pb$	±2σ	$^{238}U/^{204}Pb$	$^{235}U/^{204}Pb$	$^{232}Th/^{204}Pb$	$^{206}Pb/^{204}Pb_i$	$^{207}Pb/^{204}Pb_i$	$^{208}Pb/^{204}Pb_i$
PK1(Pankou)	10.11	20.44	1.06	18.921	0.001	15.714	0.001	38.929	0.002	35.091	0.255	3.691	17.815	15.659	38.892
PK2(Pankou)	12.44	44.56	2.27	19.691	0.001	15.71	0.001	38.667	0.002	19.787	0.144	3.642	19.067	15.679	38.631
PK3(Pankou)	5.31	8.55	4.29	19.078	0.002	15.69	0.002	38.7	0.004	44.08	0.32	35.886	17.689	15.62	38.343
PK4(Pankou)	6.11	12.81	0.31	18.911	0.002	15.647	0.002	38.434	0.004	33.846	0.245	1.751	17.844	15.594	38.417
PK5(Pankou)	3.02	17.03	0.53	19.197	0.002	15.699	0.002	38.644	0.004	12.577	0.091	2.238	18.801	15.679	38.622
PK6(Pankou)	4.81	18.02	2.12	18.713	0.002	15.658	0.002	38.614	0.004	18.921	0.137	8.386	18.117	15.628	38.531
PK7(Pankou)	5.29	12.84	0.67	18.86	0.002	15.673	0.001	38.657	0.003	29.238	0.212	3.705	17.939	15.627	38.62
PK8(Pankou)	7.25	24.44	0.79	19.243	0.002	15.687	0.002	38.599	0.004	21.05	0.153	2.303	18.58	15.654	38.576
PK9(Pankou)	6.06	20.28	1.6	18.917	0.002	15.668	0.002	38.623	0.004	21.175	0.154	5.64	18.25	15.635	38.567
PK10(Pankou)	6.71	8.32	1.32	19.534	0.002	15.693	0.002	38.479	0.004	57.183	0.415	11.3	17.732	15.603	38.367
PK11(Pankou)	2.13	22.01	0.43	19.908	0.001	15.728	0.001	38.653	0.002	6.854	0.05	1.401	19.692	15.717	38.639
PK14(Pankou)	5.31	19.03	0.74	18.819	0.001	15.671	0.001	38.675	0.001	19.804	0.144	2.782	18.195	15.64	38.647
PANK2(Pukouling)	2.85	13.0	2.09	19.005	0.001	15.726	0.001	38.851	0.002	14.130	0.102	10.707	18.560	15.704	38.744
PANK5(Pukouling)	4.89	46.8	1.64	18.710	0.001	15.712	0.001	38.812	0.002	6.703	0.049	2.323	18.499	15.701	38.789
PKZW1(Pukouling)	14.6	39.1	3.05	19.103	0.001	15.730	0.001	38.834	0.003	24.094	0.175	5.201	18.344	15.692	38.782
PKZW2(Pukouling)	8.74	35.5	1.67	18.964	0.001	15.716	0.001	38.814	0.002	15.849	0.115	3.129	18.465	15.691	38.783

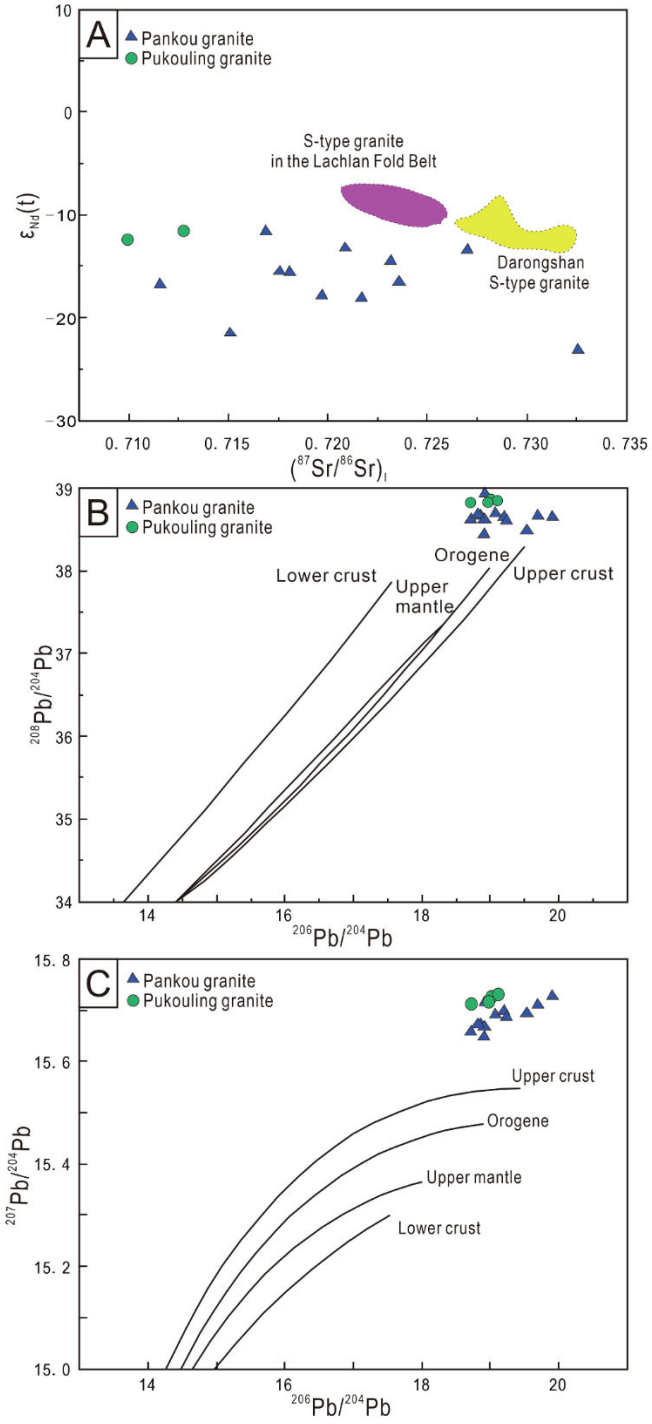

Fig. 8. Plots of (A) εNd(t) vs. $(^{87}Sr/^{86}Sr)_i$, (B) $^{208}Pb/^{204}Pb$ vs. $^{206}Pb/^{204}Pb$, and (C) $^{207}Pb/^{204}Pb$ vs. $^{206}Pb/^{204}Pb$ for the Pankou and Pukouling granites.

In addition to the REE tetrad effect, both granites are strongly depleted in Eu with most Eu/Eu* <0.39. In general, Eu is preferentially incorporated into feldspar during crystallization (Drake and Weill, 1975). Therefore, the Eu depletion of both granites provides further evidence for significant fractional crystallization.

4.3. Formation of W–Sn–Be mineralization and its relationship to the Pankou and Pukouling granites

In the Xuebaoding deposit, most coarse-grained crystals, such as beryl, scheelite, cassiterite, apatite, and fluorite, have high W, Sn, Be, B,

Table 8
LA-MC-ICPMS boron isotopic analyses of tourmalines from the Pankou and Pukouling granites, Sichuan Province, SW China.

Sample	$(^{11}B/^{10}B)_{measured}$	SE	Fractionation factor	$(^{11}B/^{10}B)_{corrected}$	$\delta^{11}B/‰$	SE
Tourmaline in Pankou and Pukouling granites (Type I tourmaline)						
XBD1-1–1	4.549	0.0002	1.137	4.001	−11.91	0.05
XBD1-1–2	4.549	0.0002	1.137	4.001	−11.88	0.04
XBD1-1–4	4.549	0.0002	1.137	4.001	−11.91	0.04
XBD1-1–5	4.548	0.0002	1.137	4.001	−11.96	0.05
XBD2-3–1	4.548	0.0002	1.137	4.001	−11.95	0.04
XBD2-3–4	4.545	0.0002	1.137	3.998	−12.58	0.04
XBD2-3–6	4.542	0.0002	1.137	3.995	−13.30	0.04
XBD2-3–7	4.540	0.0002	1.137	3.994	−13.65	0.04
XBD2-3–8	4.547	0.0002	1.137	4.000	−12.01	0.04
XBD2-3–9	4.542	0.0002	1.137	3.996	−13.18	0.05
Tourmaline from the edge of Pankou and Pukouling granites (Type II tourmaline)						
TUR5-2–1	4.563	0.0002	1.140	4.004	−11.23	0.05
TUR5-2–2	4.563	0.0002	1.140	4.004	−11.21	0.04
TUR5-2–3	4.563	0.0002	1.140	4.003	−11.30	0.04
TUR5-2–4	4.562	0.0002	1.140	4.003	−11.41	0.05
TUR5-2–5	4.559	0.0002	1.140	4.000	−12.03	0.05
TUR5-2–6	4.561	0.0002	1.140	4.002	−11.72	0.05
TUR5-2–7	4.559	0.0003	1.140	4.000	−11.98	0.05
TUR5-2–8	4.560	0.0002	1.140	4.001	−11.82	0.05
TUR5-2–9	4.558	0.0002	1.140	3.999	−12.40	0.04
TUR5-2–10	4.561	0.0002	1.140	4.002	−11.58	0.05
Tourmaline in the ore veins (Type III tourmaline)						
XBDTUR-1–13	4.566	0.0003	1.143	3.995	−13.24	0.06
XBDTUR-1–14	4.568	0.0002	1.143	3.996	−12.97	0.05
XBDTUR-1–15	4.568	0.0003	1.143	3.997	−12.89	0.06
XBDTUR-1–16	4.567	0.0002	1.143	3.996	−13.06	0.05
XBDTUR-1–17	4.569	0.0003	1.143	3.998	−12.72	0.05
XBDTUR-1–18	4.570	0.0003	1.143	3.999	−12.41	0.05
XBDTUR-1–19	4.570	0.0003	1.143	3.999	−12.42	0.06
XBDTUR-1–20	4.571	0.0002	1.143	4.000	−12.13	0.05
XBDTUR-1–21	4.570	0.0003	1.143	3.998	−12.50	0.06
XBDTUR-1–22	4.567	0.0003	1.143	3.996	−13.00	0.06

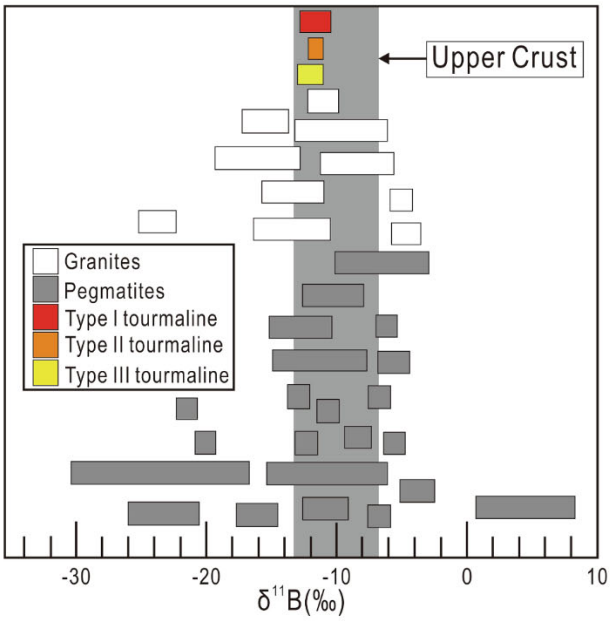

Fig. 9. $\delta^{11}B$ values of tourmaline in the Xuebaoding deposit compared with compiled data for other granites and pegmatites worldwide. The shaded bar is the range for average upper crust (modified after Trumbull et al., 2008).

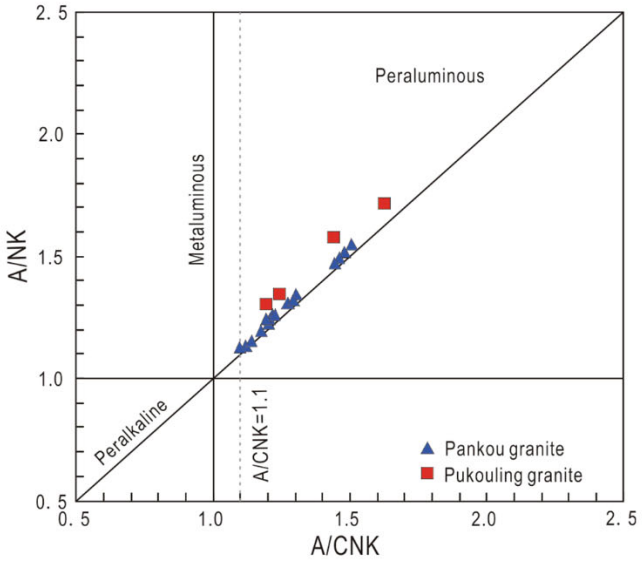

Fig. 10. Plot of A/NK ($Al_2O_3/[Na_2O + K_2O]$) vs. A/CNK ($Al_2O_3/[CaO + Na_2O + K_2O]$) (Maniar and Piccoli, 1989) for the Pankou and Pukouling granites.

P, F, Li, Rb, and Cs contents. Given that K-feldspar occurs mainly in Zone I without large amounts of W–Sn–Be-bearing minerals, while albite is closely associated with beryl, fluorite, cassiterite, and scheelite in Zone III. It is clear that the ore-forming fluids evolved from K- to Na-rich. Albite inclusions in K-feldspar in Zone I indicate the former began to form by solid solution processes. This occurred from 600 to 500 °C during pegmatite formation (Liu, 2017). Then, the K-feldspar represents the pegmatite stage with limited W–Sn–Be mineralization. This stage occurred after magma crystallization in Zone I, and prior to mineralization in Zone III. During beryl, scheelite, apatite, and tourmaline mineralization, tabular albite formed instead of K-feldspar (Fig. 3). This is consistent with microthermometric measurements of fluid inclusions in beryl, cassiterite, scheelite, and quartz (homogenization temperatures of 201–332 °C; Liu et al., 2012a). Therefore, the transition from the pegmatite to hydrothermal stage was accompanied by a decrease in

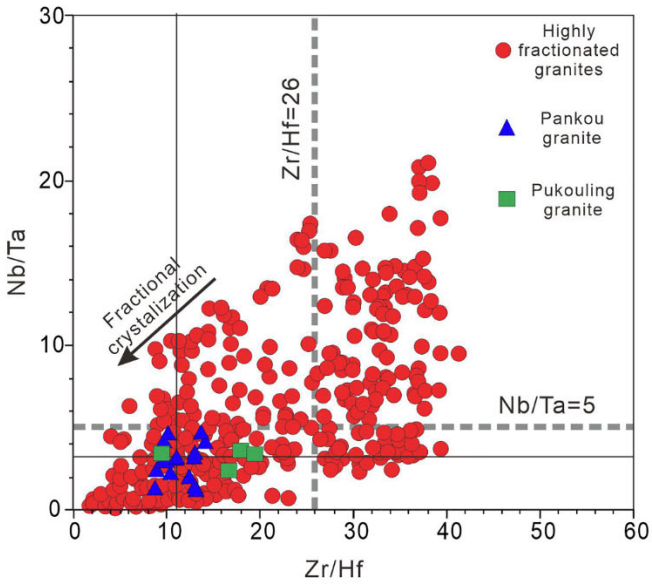

Fig. 11. Plot of Nb/Ta vs. Zr/Hf for the Pankou and Pukouling granites (modified after Wu et al., 2017).

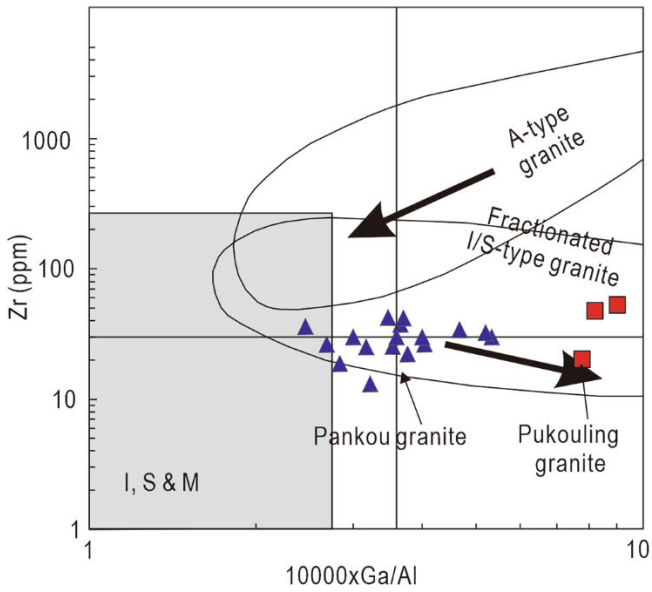

Fig. 12. Discrimination diagram for A-, fractionated I-, and S-type granites, which shows data for the Pankou and Pukouling granites. The diagram is based on those of Whalen et al. (1987) and Wu et al. (2017).

temperature and K contents, and an increase in Na contents, in the ore-forming fluids (Liu, 2017).

Tabular beryl crystals in the Xuebaoding deposit have high alkali contents, including Li_2O (2.60–3.10 wt%), Rb (65–120 ppm), Cs_2O (0.70–0.92 wt%), and Na_2O (1.29–1.66 wt%). These are characteristics of Na–Li–Cs beryl, which is dominated by tetrahedral substitution in the crystal structure, with Li^+ in the tetrahedral site and Li^+, Na^+, K^+, and Cs^+ in structural channels (Liu et al., 2012b).

Scheelite in the studied granites contains a larger amount of REEs (369–1171 ppm) than in other ore deposits (e.g., Brugger et al., 2002; Gu et al., 2006; Roberts et al., 2006). The REEs are located in the Ca^{2+} site of the scheelite crystal structure (Ghaderi et al., 1999; Brugger et al., 2000).

Tourmaline crystals in the ore veins are acicular and Al- and B-rich. Although these tourmalines are classified as foitite and schorl, they have a high Al content. The low Na contents and high Fe^{3+}/Fe^{2+} ratios of the tourmaline crystals indicate the ore-forming fluids were oxidized and low-salinity (Zhu et al., 2020).

In general, the occurrence of apatite and fluorite, along with beryl, scheelite, cassiterite, and tourmaline, suggests that Xuebaoding deposit containing these minerals are rich in W, Sn, Be, Li, Na, K, Rb, F, B, P, and Cs. The marble in the Xuebaoding deposit has low W, Sn, Be, Li, Rb, and Cs concentrations. Hence, these trace and ore elements were derived from the granites rather than the marble as no other rocks occur around the Xuebaoding deposit. However, given that quartz, muscovite, and albite do not contain these trace and ore elements, these elements became enriched in magmatic–hydrothermal fluids.

In most W–Sn ore deposits, alteration is pronounced and results in greisen and skarn formation (Mao et al., 2019), especially in some large deposits such as those at Shizhuyuan (Lu et al., 2003), Xihuashan (Xu and Li, 2013), and Baiganhu (Gao et al., 2014). However, the Xuebaoding deposit exhibits little alteration, but still contains well-developed W–Sn–Be mineralization. This is possibly due to three factors: (1) the highly fractionated granites provided sufficient rare-metals and resulted in enrichment of W, Sn, and Be during the magmatic–hydrothermal evolution of the granitic system; (2) the low mineralization temperatures and limited fluid–rock interactions might have been caused by the occurrence of large fractures; (3) the different crystal nature of the rock-forming minerals such as muscovite, quartz and K-feldspar cannot accommodate W, Sn, Be or large amounts of alkali elements. Other factors that facilitate W–Sn–Be enrichment have been summarized in Liu et al. (2012a): marble and calcic schist as the main host rocks provided the Ca for the formation of scheelite, fluorite, calcite, and apatite. The reaction between marble and ore-forming fluids accelerated the W-Sn-Be mineralization. In addition, fluid immiscibility can occur during the pressure decrease induced by formation of extensional joints, which facilitated the Zone III mineralization.

5. Conclusions

(1) The Pankou and Pukouling granites are highly fractionated S-type granites that were derived by partial melting of an upper crustal source.

(2) In the Xuebaoding deposit, W–Sn–Be mineralization occurred at low temperatures and was associated with limited alteration. The high W, Sn, and Be contents in the highly fractionated granites and enrichment of these elements during magmatic–hydrothermal process led to mineralization.

Declaration of Competing Interest

The authors declare that they have no known competing financial interests or personal relationships that could have appeared to influence the work reported in this paper.

Acknowledgements

We are grateful to two anonymous reviewers who provided constructive suggestions on this manuscript. This research was funded by the Strategic Priority Research Program of the Chinese Academy of Sciences (Grant XDA20070304), National Natural Science Foundation of China (Grants 41572113, 41772044, and 41922014), Fundamental Research Funds for the Institute of Geology, Chinese Academy of Geological Sciences (Grant J2004), China Geological Survey, Ministry of Natural Resources (Grants DD20190060 and DD20211358), and Key Special Project for Introduced Talents Team of Southern Marine Science and Engineering, Guangdong Laboratory (Guangzhou) (Grant GML2019ZD0106).

Appendix A. Supplementary data

Supplementary data to this article can be found online at https://doi.org/10.1016/j.oregeorev.2021.104197.

References

Anglin, C.D., Jonasson, I.R., Franklin, J.M., 1996. Sm-Nd dating of scheelite and tourmaline: Implications for the genesis of Archean gold deposits, Val d'Or, Canada. Econ. Geol. 91, 1372–1382.

Audétat, A., Günther, D., Heinrich, C.A., 2000. Magmatic-hydrothermal evolution in a fractionating granite: A microchemical study of the Sn-W- F- mineralized Mole Granite (Australia). Geochim. Cosmochim. Acta 64, 3373–3393.

Aurisicchio, C., Fioravanti, G., Grubessi, O., Zanazzi, P.F., 1988. Reappraisal of the crystal chemistry of beryl. Am. Mineral. 73, 826–837.

Bettencourt, J.S., Leute Jr., W.B., Goraieb, C.L., Sparrenberger, I., Bello, R.M.S., Payolla, B.L., 2005. Sn-polymetallic greisen-type deposits associated with late-stage rapakivi granites, Brazil: fluid inclusion and stable isotopes characteristics. Lithos 80, 363–386.

Breiter, K., Müller, A., Leichmann, J., Gabašová, A., 2005. Textural and chemical evolution of a fractionated granitic system: the Podlesí stock, Czech Republic. Lithos 80, 323–345.

Brugger, J., Lahaye, Y., Costa, S., Lambert, D., Bateman, R., 2000. Inhomogeneous distribution of REE in scheelite and dynamics of Archaean hydrothermal systems (Mt Charlotte and Drysdale gold deposits, Western Australia). Contrib. Miner. Petrol. 139, 251–264.

Brugger, J., Maas, R., Lahaye, Y., McRae, C., Ghaderi, M., Costa, S., Lambert, D., Bateman, R., Prince, K., 2002. Origins of Nd- Sr- Pb isotopic variations in single scheelite grains from Archaean gold deposits, Western Australia. Chem. Geol. 182, 203–225.

Cao, Z.M., Zheng, J.B., Li, Y.G., Ren, J.G., Xu, S.J., Wang, R.C., Shoji, T., Kaned, H., Kabayashi, S., 2002. Geologic and geochemical features of the volatile-rich ore fluid and its tracing and dating in the Xuebaoding Beryl-Scheelite Vein Deposit, China. Science in China 45, 719–729.

Cao, Z.M., Zheng, J.P., An, W., Li, Y.G., 2004. Geochemistry of Xuebaoding alkali granite and its ore-controlling effect. Journal of Ocean University of Qingdao 34, 874–880 (in Chinese with English abstract).

Chappell, B.W., 1999. Aluminium Saturation in I- and S- Type Granites and the Characterization of Fractionated Haplogranites. Lithos 46 (3), 535–551.

Chappell, B.W., White, A.J.R., 1974. Two contrasting granite types. Pac. Geol. 8, 173–174.

Chappell, B.W., White, A.J.R., 1992. I- and S-type granites in the Lachlan Fold Belt. Transactions of the Royal Society of Edinburgh: Earth Sciences 83, 1–26.

Clemens, J.D., 2003. S-type granitic magmas-petrogenetic issues, models and evidence. Earth Sci. Rev. 61 (1–2), 1–18.

Collins, W.J., Beams, S.D., White, A.J.R., Chappell, B.W., 1982. Nature and Origin of a-Type Granites with Zoneicular Reference to Southeastern Australia. Contrib. Miner. Petrol. 80 (2), 189–200.

Collins, W.J., Richards, S.W., 2008. Geodynamic significance of S-type granites in circum-Pacific orogens. Geology 36 (7), 559–562.

Cuney, M., Marignac, C., Weisbrod, A., 1992. The Beauvoir topaz-lepidolite albite granite (Massif Central, France); the disseminated magmatic Sn-Li-Ta-Nb-Be mineralization. Econ. Geol. 87, 1766–1794.

Dingwell, D.B., Pichavant, M., Holtz, F., 1996. Experimental studies of boron in granitic melts. Rev. Mineral. 33, 331–385.

Drake, M.J., Weill, D.F., 1975. Partition of Sr, Ba, Ca, Y, Eu^{2+}, Eu^{3+}, and other REE between plagioclase feldspar and magmatic liquid: an experimental study. Geochim. Cosmochim. Acta 39 (5), 689–712.

Drivenes, K., Larsen, R.B., Müller, A., Sørensen, B.E., Wiedenbeck, M., Raanes, M.P., 2015. Late-magmatic immiscibility during batholith formation: Assessment of B isotopes and trace elements in tourmaline from the Land's End granite, SW England. Contrib. Miner. Petrol. 169, 56.

Duc-Tin, Q., Audétat, A., Keppler, H., 2007. Solubility of tin in (Cl, F)-bearing aqueous fluids at 700°C,140 MPa: A LA- ICP- MS study on synthetic fluid inclusions. Geochim. Cosmochim. Acta 71, 3323–3335.

Eby, G.N., 1990. The a-Type Granitoids - a Review of Their Occurrence and Chemical Characteristics and Speculations on Their Petrogenesis. Lithos 26 (1–2), 115–134.

Eby, G.N., 1992. Chemical Subdivision of the a-Type Granitoids - Petrogenetic and Tectonic Implications. Geology 20 (7), 641–644.

Esmaeily, D., Nédélecb, A., Valizadeh, M.V., Moorec, F., Cottend, J., 2005. Petrology of the Jurassic Shah-Kuh granite (eastern Iran), with reference to tin mineralization. J. Asian Earth Sci. 25, 961–980.

Frost, C.D., Frost, B.R., 2011. On Ferroan (A-type) Granitoids: their Compositional Variability and Modes of Origin. J. Petrol. 52 (1), 39–53.

Gaans, P.F.M., van Vriend, S.P., Poorter, R.P.E., 1995. Hydrothermal processes and shifting element associated patterns in the W-Sn enriched granite of Regoufe, Portugal. J. Geochem. Explor. 55, 203–222.

Gao, Y.B., Li, W.Y., Li, Z.M., Wang, J., Hattori, K., Zhang, Z.W., Geng, J.Z., 2014. Geology, geochemistry, and genesis of tungsten-tin deposits in the Baiganhu district, northern Kunlun belt, northwestern, China. Econ. Geol. 109, 1787–1799.

Garda, G.M., Trumbull, R.B., Beljavskis, P., Wiedenbeck, M., 2009. Boron isotope composition of tourmalinite and vein tourmalines associated with gold mineralization, Serra do Itaberaba Group, central Ribeira Belt, SE Brazil. Chemical Geology 264 (1–4), 207–220.

Gavrilenko, E.V., Pérez, B. Calvo, Bolibar, R. Castroviejo, del Amo, D., García, 2006. Emeralds from the Delbegetey deposit (Kazakhstan): mineralogical characteristics and fluid-inclusion study. Mineral. Mag. 70, 159–173.

Gelman, S.E., Deering, C.D., Bachmann, O., Huber, C., Gutiérrez, F.J., 2014. Identifying the crystal graveyards remaining after large silicic eruptions. Earth Planet. Sci. Lett. 403, 299–306.

Geology and Mineral Resource Bureau of Sichuan Province, 1975. Regional Survey Report of Songpan Sheet at the 1:200,000 Scalegeology in Sichuan Province. Whole report not acquired (in Chinese).

Ghaderi, M., Palin, J.M., Campbell, I.H., Sylvester, P.J., 1999. Rare earth element systematics in scheelite from hydrothermal gold deposits in the Kalgoorlie-Norseman region, western Australia. Econ. Geol. 94, 423–438.

Gill, T. B., 1981. Orogenic Andesite and Plate Tectonics: Berlin, Springer-Verlag, 390.

Groat, L.A., Giuliani, G., Marshall, D.D., Turner, D., 2008. Emerald deposits and occurrences: A review. Ore Geol. Rev. 34, 87–112.

Groat, L.A., Marshall, D.D., Giuliani, G., Murphy, D.C., Piercey, S.J., Jambor, J.L., Mortensen, J.K., Ercit, T.S., Gault, R.A., Mattey, D.P., Schwartz, D., Maluski, H., Wise, M.A., Wengzynowski, W., Eaton, D.W., 2002. Mineralogical and geochemical study of the Regal Ridge emerald showing, Southern Yukon. The Canadian Mineralogist 40, 1313–1338.

Gu, X.X., Schulz, O., Vavtar, F., Liu, J.M., Zheng, M.H., Fu, S.H., 2006. Rare earth element geochemistry of the Woxi W- Sb- Au deposit, Hunan Province, South China. Ore Geol. Rev. 31, 319–336.

Hervig, R.L., Moore, G.M., Williams, L.B., Peacock, S.M., Holloway, J.R., Roggensack, K., 2002. Isotopic and element Zoneitioning of boron between hydrous fluid and silicate melt. Am. Mineral. 87, 769–774.

Hineab, R., Williamscd, I.S., Chappelle, B.W., White, A.J.R., 1978. Contrasts between I- and S- type granitoids of the Kosciusko Batholith. J. Geol. Soc. Aust. 25 (3–4), 219–234.

Hu, Z.C., Gao, S., 2008. Upper crustal abundances of trace elements: A revision and update. Chem. Geol. 253, 205–221.

Huang, S., Song, Y., Hou, Z., Xue, C., 2016. Chemical and stable isotopic (B, H, and O) compositions of tourmaline in the Maocaoping vein-type Cu deposit, western Yunnan, China: Constraints on fluid source and evolution. Chem. Geol. 439, 173–188.

Jiang, S.Y., Radvanec, M., Nakamura, E., Palmer, M., Kobayashi, K., Zhao, H.X., Zhao, K. D., 2008. Chemical and boron isotopic variations of tourmaline in the Hnilec granite-related hydrothermal system, Slovakia: Constraints on magmatic and metamorphic fluid evolution. Lithos 106, 1–11.

Keppler, H., Wyllie, P.J., 1991. Zoneitioning of Cu, Sn, Mo, W, U and Th between melt and aqueous fluid in the systems haplogranite- H_2O- HF. Contrib. Miner. Petrol. 109, 139–150.

Lee, C.T.A., Morton, D.M., 2015. High silica granites: Terminal porosity and crystal settling in shallow magma chambers. Earth Planet. Sci. Lett. 409, 23–31.

Lenharo, S.R.L., Moura, M.A., Botelho, N.F., 2002. Petrogenetic and mineralization processes in Paleo- to Mesoproterozoic rapakivi granites: examples from Pitinga and Goias, Brazil. Precambr. Res. 119, 277–299.

Li, J.K., Liu, S.B., Wang, D.H., Fu, X.F., 2007. Metallogenic epoch of Xuebaoding W- Sn-Be deposit in northwest Sichuan and its tectonic tracing significance. Mineral deposits 26, 557–562 (in Chinese with English abstract).

Li, J., Huang, X.L., 2013. Mechanism of Ta-Nb enrichment and magmatic evolution in the Yashan granites, Jiangxi Province, south China (in Chinese). Acta Petrologica Sinica 29, 4311–4322.

Li, J., Huang, X.L., He, P.L., Li, W.X., Yu, Y., Chen, L., 2015. In situ analyses of micas in the Yashan granite, South China: Constraints on magmatic and hydrothermal evolutions of W and Ta-Nb bearing granites. Ore Geol. Rev. 65, 793–810.

Li, Y.L., Zhang, H.F., Guo, J.H., Li, C.F., 2017. Petrogenesis of the Huili Paleoproterozoic leucogranite in the Jiaobei Terrane of the North China Craton: A highly fractionated albite granite forced by K-feldspar fractionation. Chem. Geol. 450, 165–182.

Linnen, R.L., 1998. The solubility of Nb- Ta- Zr- Hf- W in granitic melts with Li and Li+ F: Contraints for mineralization in rare metal granites and pegmetites. Econ. Geol. 93, 1013–1025.

Liu, Y., Hou, Z.Q., 2017. A synthesis of mineralization styles with an integrated genetic model of carbonatite-syenite-hosted REE deposits in the Cenozoic Mianning-Dechang REE metallogenic belt, the eastern Tibetan Plateau, southwestern China. J. Asian Earth Sci. 137, 35–79.

Liu, C.S., Ling, H.F., Xiong, X.L., Shen, W.Z., Wang, D.Z., Huang, X.L., Wang, R.C., 1999. An F- rich, Sn- bearing volcanic- intrusive complex in Yanbei, South China. Econ. Geol. 94, 325–342.

Liu, Y., 2010. Mineralogical characteristics and formation mechanism of Xuebaoding W-Sn-Be deposit in Northwest Sichuan. China University of Geosciences (Beijing). Ph.D Dissertation.

Liu, Y., 2017. Mineralogical characteristics and genetic mechanism of the Xuebaoding deposit in northwestern Sichuan Province. Journal of rock mineralogy 36 (04), 549–563 (Chinese in English abstract).

Liu, Y., Chakhmouradian, A.R., Hou, Z.Q., Song, W.L., Kynický, J., 2019a. Development of REE mineralization in the giant Maoniuping deposit (Sichuan, China): insights from mineralogy, fluid inclusions, and trace-element geochemistry. Miner. Deposita 54, 701–718.

Liu, Y., Deng, J., Li, C.F., Shi, G.H., Zheng, A.L., 2007a. REE composition in scheelite and scheelite Sm- Nd dating for the Xuebaoding W-Sn-Be deposit in Sichuan. Chin. Sci. Bull. 52, 2543–2550.

Liu, Y., Deng, J., Li, G., Shi, G., 2007b. Structure Refinement of Cs- rich and Na-Li Beryl and Analysis of Its Typomorphic Characteristic of Configurations. Acta Geol. Sin. 81, 61–67.

Liu, Y., Deng, J., Shi, G.H., Sun, D.S., 2012a. Geochemical and Morphological Characteristics of Coarse-grained Tabular Beryl from the Xuebaoding W-Sn-Be deposit, Sichuan Province. Western China. International Geology Review 54 (14), 1673–1684.
Liu, Y., Deng, J., Shi, G., Sun, X., Yang, L., 2012b. Genesis of the Xuebaoding W-Sn-Be crystal deposits in southwest China: evidence from fluid inclusions, stable isotopes and ore elements. Resour. Geol. 62 (2), 159–173.
Liu, Y., Deng, J., Sun, D., Zhou, Y., 2007c. Morphology and Gensis Typomorphism of Minerals in W-Sn-Be Deposit of Huya, Sichuan. Editorial Committee of Earth Science-Journal of China University of Geosciences 32, 75–81 (in Chinese with English abstract).
Liu, Y., Deng, J., Zhang, G.B., Shi, G.H., Yang, L.Q., Wang, Q.F., 2010. $^{40}Ar/^{39}Ar$ Dating of Xuebaoding Granite in the Songpan-Garzê Orogenic Belt, Southwest China, and its Geological Significance. Acta Geologica Sinica English Edition 84, 345–357.
Liu, Y., Hou, Z.Q., Zhang, R.Q., Wang, P., Gao, J.F., Raschke, M.B., 2019b. Zircon Alteration as a Proxy for Rare Earth Element Mineralization Processes in Carbonatite-Nordmarkite Complexes of the Mianning-Dechang Rare Earth Element Belt, China. Econ. Geol. 114, 719–744.
Liu, Z.C., Wu, F.Y., Ding, L., Liu, X.C., Wang, J.G., Ji, W.Q., 2016. Highly fractionated late Eocene (~35 Ma) leucogranite in the Xiaru dome, Tethyan Himalaya, South Tibet. Lithos 240, 337–354.
London, D., 1992. The application of experimental petrology to the genesis and crystallization of granitic pegmatites. Can. Mineral. 30, 499–540.
London, D., Evensen, J. M., 2002. Beryllium in silicic magmas and the origin of Beryl-bearing pegmatites. In: Grew E S, ed. Beryllium: Mineralogy, Petrology, and Geochemistry. Reviews in Mineralogy & Geochemistry, 50, 445–486.
Longfellow, K.M., Swanson, S.E., 2011. Skeletal tourmaline, undercooling, and crystallization history of the Stone Mountain granite, Georgia, USA. Can. Mineral. 49, 341–357.
Lu, H.Z., Liu, Y., Wang, C., Xu, Y., Li, H., 2003. Mineralization and Fluid Inclusion Study of the Shizhuyuan W- Sn- Bi- Mo- F Skarn Deposit, Hunan Province, China. Econ. Geol. 98, 955–974.
Macey, P., Harris, C., 2006. Stable isotope and flfuid inclusion evidence for the origin of the Brandberg West area Sn-W vein deposits, NW Namibia. Miner. Deposita 41, 671–690.
Maniar, P.D., Piccoli, P.M., 1989. Tectonic discrimination of granitoids. Geol. Soc. Am. Bull. 101, 635–643.
Mao, J.W., Ouyang, H.G., Santosh, M., Yuan, S.D., Zhou, Z.H., Zheng, W., Liu, H., Liu, P., Chen, M.H., 2019. Geology and Metallogeny of Tungsten and Tin Deposits in China. SEG Special Publications 22, 411–482.
Marshall, D.D., Groat, L.A., Falck, H., Giuliani, G., Neufeld, H., 2004. The Lened emerald prospect, Northern Territories, Canada: Insights from fluid inclusions and stable isotopes, with implications for Northern Cordilleran emeralds. Can. Mineral. 42, 1523–1539.
Marshall, D.D., Groat, L.A., Giuliani, G., Murphy, D., Mattey, D., Ercit, T.S., Wise, M.A., Wengzynowski, W., Eaton, W.D., 2003. Pressure, temperature and fluid conditions during emerald precipitation, southeastern Yukon, Canada: fluid inclusion and stable isotope evidence. Chem. Geol. 193, 187–199.
McDonough, W.F., Sun, S.S., 1995. The composition of the Earth. Chem. Geol. 120, 223–253.
Middlemost, E.A.K., 1994. Naming materials in the magma igneous rock system. Earth Sci. Rev. 37, 215–224.
Morgan, V.I.G.B., London, D., Kirkpatrick, R.J., 1990. Reconnaissance spectroscopic study of hydrous sodium aluminum borosilicate glasses. Geological Society of America Abstracts with Programs 22, A167.
Neiva, A.M.R., 2008. Geochemistry of cassiterite and wolframite from tin and tungsten quartz veins in Portugal. Ore Geol. Rev. 33, 221–238.
Pal, D.C., Mishra, B., Bernhardt, H.J., 2007. Mineralogy and geochemistry of pegmatite-hosted Sn-, Ta- Nb-, and Zr- Hf- bearing minerals from the southeastern Zone of the Bastar-Malkangiri pegmatite belt, Central Inida. Ore Geol. Rev. 30, 30–55.
Palmer, M.R., London, D., Morgan, V.I.G.B., Babb, H.A., 1992. Experimental determination of fractionation of $^{11}B/^{10}B$ between tourmaline and aqueous vapor. A temperature and pressure-dependent isotopic system. Chem. Geol. 101, 123–129.
Palmer, M.R., Swihart, G.H., 1996. Boron isotope geochemistry: an overview. Rev. Mineral. Geochem. 33, 709–744.
Pettke, T., Audétat, A., Schaltegger, U., Heinrich, C.A., 2005. Magmatic to hydrothermal crystallization in the W-Sn mineralized Mole Granite (NSW, Australia): Zone II: Evolving zircon and thorite trace element chemistry. Chem. Geol. 220, 191–213.
Raimbault, I., Cuney, M., Azancott, C., Douthou, J.L., Joron, J.L., 1995. Geochemical evidence for a multistage genesis of Ta-Sn-Li mineralization in the granite at Beauvoir, French massif Central. Econ. Geol. 90, 548–576.
Rakovan, J.A., 2007. Word to Wise: Greisen. Rocks Miner. 82, 157–159.
Roberts, M.P., Clemens, J.D., 1993. Origin of High-Potassium, Calc-Alkaline. I-Type Granitoids. Geology 21 (9), 825–828.
Roberts, S., Palmer, M.R., Waller, L., 2006. Sm- Nd and REE characteristics of tourmaline and scheelite from the Bjorkdal gold deposit, northern Sweden: Evidence of an intrusion-related gold deposit. Econ. Geol. 101, 1415–1425.
Rozendaal, A., Bruwer, L., 1995. Tourmaline nodules: Indicators of hydrothermal alteration and Sn-Zn-(W) mineralization in the Cape Granite Suite, South Africa. J. Afr. Earth Sc. 21, 141–155.
Samson, I.M., Sinclair, W.D., 1992. Magmatic hydrothermal fluids and the origin of quartz-tourmaline orbicules in the Seagull batholith. Yukon Territory. The Canadian Mineralogist 30 (3), 937–954.
Sirbescu, M.-L.C., Nabelek, P.I., 2003. Crustal melts below 400 °C. Geology 31, 685–688.
Somarin, A.K., Ashley, A., 2004. Hydrothermal alteration and mineralization of the Glen Eden Mo- W- Sn deposit: a leucogranite-related hydrothermal system, Southern New England Orogen, NSW, Australia. Miner. Deposita 39, 282–300.
Thomas, R., Förster, H.J., Heinrich, W., 2003. The behavior of boron in a peraluminous granite-pegmatite system and associated hydro- thermal solutions: a melt and fluid inclusion study. Contrib. Miner. Petrol. 144, 457–472.
Thomas, R., Förster, H.J., Rickers, K., Webster, J.D., 2005. Formation of extremely hydrous melt fractions and hydrothermal fluids during differentiation of highly evolved tin-granite magmas: a melt/fluid inclusion study. Contrib. Miner. Petrol. 148, 582–601.
Tonarini, S., Forte, C., Petrini, R., Ferrara, G., 2003. Melt/biotite $^{11}B/^{10}B$ isotopic fractionation and the boron local environment in the structure of volcanic glasses. Geochim. Cosmochim. Acta 67, 1863–1873.
Trumbull, R.B., Krienitz, M.S., Gottesmann, B., Wiedenbeck, M., 2008. Chemical and boron-isotope variations in tourmalines from an S-type granite and its source rocks: the Erongo granite and tourmalinites in the Damara Belt. Namibia. Contributions to Mineralogy and Petrology 155 (1), 1–18.
Vapnik, Y., Moroz, I., Roth, M., Eliezri, I., 2006. Formation of emeralds at pegmatite-ultramafic contacts based on fluid inclusions in Kianjavato emerald, Mananjary deposits, Madagascar. Mineral. Mag. 70, 141–158.
Veksler, I.V., Thomas, R., 2002. An experimental study of B-, P- and F- rich synthetic granite pegmatite at 0.1 and 0.2 GPa. Contrib. Miner. Petrol. 143, 673–683.
Wang, R.C., Che, X.D., Zhang, W.L., Zhang, A.C., Zhang, H., 2009. Geochemical evolution and late re-equilibration of Na-Cs-rich beryl from the Koktokay #3 pegmatite (Altai, NW China). Eur. J. Mineral. 21, 795–809.
Wang, X.L., Zhou, J.C., Wan, Y.S., Kitajima, K., Wang, D., Bonamici, C., 2013. Magmatic evolution and crustal recycling for Neoproterozoic strongly peraluminous granitoids from southern China: Hf and O isotopes in zircon. Earth Planet. Sci. Lett. 366, 71–82.
Wedepohl, K.H., 1995. The composition of the continental crust. Geochim. Cosmochim. Acta 59, 1217–1232.
Whalen, J.B., Currie, K.L., Chappell, B.W., 1987. A-type granites: Geochemical characteristics, discrimination and petrogenesis. Contrib. Miner. Petrol. 95, 407–419.
Williams, L.B., Hervig, R.L., Holloway, J.R., Hutcheon, I., 2001. Boron isotope geochemistry during diagenesis. Part I. Experimental determination of fractionation during illitization of smectite. Geochim. Cosmochim. Acta 65, 1769–1782.
Wu, F.Y., Jahn, B.M., Wilde, S.A., Lo, C.H., Yui, T.F., Lin, Q., Ge, W.C., Sun, D.Y., 2003a. Highly fractionated I-type granites in NE China (I): geochronology and petrogenesis. Lithos 66 (3–4), 241–273.
Wu, F.Y., Jahn, B.M., Wilde, S.A., Lo, C.H., Yui, T.F., Lin, Q., Ge, W.C., Sun, D.Y., 2003b. Highly fractionated I-type granites in NE China (II): isotopic geochemistry and implications for crustal growth in the Phanerozoic. Lithos 67 (3–4), 191–204.
Wu, F., Liu, X., Ji, W., Wang, J., Yang, L., 2017. Highly fractionated granites: Recognition and research. Science China Earth Sciences 60 (7), 1201–1219.
Wunder, B., Meixner, A., Romer, R.L., Wirth, R., Heinrich, W., 2005. The geochemical cycle of boron: constraints from boron isotope Zoneitioning experiments between mica and fluid. Lithos 84, 206–216.
Xu, T., Li, Z.H., 2013. Characteristics of fluid inclusions and origin of ore-forming fluids in Xihuashan tungsten deposit. Jiangxi Province. Resources Survey & Environment 34 (2), 95–101 (in Chinese with English abstract).
Ye, S., Qi, L., Luo, Y., Zhou, K., Pi, J., 2001. Realationship between the rare- metal contained granitic intrusions and beryl mineralization in Pingwu, Sichuan, China. Geological ence and Technology Information 20, 65–70 (in Chinese with English abstract).
Yokart, B., Barr, S.M., Williams-Jones, A.E., Macdonald, A.S., 2003. Late- stage alteration and tin-tungsten mineralization in the Khuntan Batholith, northern Thailand. J. Asian Earth Sci. 21, 999–1018.
Zhang, A.C., Wang, R.C., Jiang, S.Y., Hu, H., Zhang, H., 2008. Chemical and textural features of tourmaline from the spodumene-subtype Koktokay no. 3 pegmatite, Altai, northwestern China: A record of magmatic to hydrothermal evolution. Can. Mineral. 46, 41–58.
Zhang, D.L., Peng, J.T., Coulson, I.M., Hou, L.H., Li, S.J., 2014. Cassiterite U-Pb and muscovite $^{40}Ar–^{39}Ar$ age constraints on the timing of mineralization in the Xuebaoding Sn-W-Be deposit, western China. Ore Geol. Rev. 62, 315–322.
Zhu, J.C., Rao, B., Xiong, X.L., Li, F.C., Zhang, P.H., 2002. Correlation and genesis of rare mineralized granitoids rich in lithium and fluorine. Geochemistry 02, 141–152 (in Chinese with English abstract).
Zhu, X., Raschke, M.B., Liu, Y., 2020. Tourmaline as a Recorder of Ore-Forming Processes in the Xuebaoding W-Sn-Be Deposit, Sichuan Province, China: Evidence from the Chemical Composition of Tourmaline. Minerals 10 (5), 438.